Quaternary Science Reviews 153 (2016) 78–96

Contents lists available at ScienceDirect

Quaternary Science Reviews

journal homepage: www.elsevier.com/locate/quascirev

Evaluating the timing of former glacier expansions in the Tian Shan: A key step towards robust spatial correlations

R. Blomdin [a, b, c, *], A.P. Stroeven [a, b], J.M. Harbor [a, b, c], N.A. Lifton [c, d], J. Heyman [e], N. Gribenski [a, b], D.A. Petrakov [f], M.W. Caffee [c, d], M.N. Ivanov [f], C. Hättestrand [a, b], I. Rogozhina [g, h], R. Usubaliev [i]

[a] Geomorphology and Glaciology, Department of Physical Geography, Stockholm University, Stockholm, Sweden
[b] Bolin Centre for Climate Research, Stockholm University, Stockholm, Sweden
[c] Department of Earth, Atmospheric, and Planetary Sciences, Purdue University, West Lafayette, USA
[d] Department of Physics and Astronomy, Purdue Rare Isotope Measurement Laboratory (PRIME Lab), Purdue University, West Lafayette, USA
[e] Department of Earth Sciences, University of Gothenburg, Gothenburg, Sweden
[f] Faculty of Geography, Lomonosov Moscow State University, Moscow, Russia
[g] MARUM, University of Bremen, Bremen, Germany
[h] German Research Centre for Geosciences, Potsdam, Germany
[i] Central Asian Institute of Applied Geosciences, Bishkek, Kyrgyzstan

ARTICLE INFO

Article history:
Received 6 April 2016
Received in revised form
28 June 2016
Accepted 25 July 2016

Keywords:
Paleoglaciation
Tian Shan
Glacial geomorphology
^{10}Be surface exposure dating

ABSTRACT

The timing of past glaciation across the Tian Shan provides a proxy for past climate change in this critical area. Correlating glacial stages across the region is difficult but cosmogenic exposure ages have considerable potential. A drawback is the large observed scatter in ^{10}Be surface exposure data. To quantify the robustness of the dating, we compile, recalculate, and perform statistical analyses on sets of ^{10}Be surface exposure ages from 25 moraines, consisting of 114 new and previously published ages. We assess boulder age scatter by dividing boulder groups into quality classes and rejecting boulder groups of poor quality. This allows us to distinguish and correlate robustly dated glacier limits, resulting in a more conservative chronology than advanced in previous publications. Our analysis shows that only one regional glacial stage can be reliably correlated across the Tian Shan, with glacier expansions occurring between 15 and 28 ka during marine oxygen isotope stage (MIS) 2. However, there are examples of older more extensive indicators of glacial stages between MIS 3 and MIS 6. Paleoglacier extent during MIS 2 was mainly restricted to valley glaciation. Local deviations occur: in the central Kyrgyz Tian Shan paleoglaciers were more extensive and we propose that the topographic context explains this pattern. Correlation between glacial stages prior to late MIS 2 is less reliable, because of the low number of samples and/or the poor resolution of the dating. With the current resolution and spatial coverage of robustly-dated glacier limits we advise that paleoclimatic implications for the Tian Shan glacial chronology beyond MIS 2 are speculative and that continued work toward robust glacial chronologies is needed to resolve questions regarding drivers of past glaciation in the Tian Shan and Central Asia.

1. Introduction

Glaciers are sensitive to changes in temperature (surface energy flux) and precipitation by expanding (due to mass gain) or receding (due to mass loss). Concordant with global trends (IPCC; Vaughan et al., 2013), glaciers in the Tian Shan in Central Asia (Fig. 1) are receding. Glacier mass balance (mass change over a year) in the Tian Shan has been highly negative due to recent increases in summer temperatures and changes in precipitation partitioning over the year (Aizen et al., 2007a; Kriegel et al., 2013; Farinotti et al., 2015). Several mountain systems are likewise experiencing glacier recession, including the Ak-Shyirak Massif (Khromova, 2003; Aizen et al., 2007b; Pieczonka and Bolch, 2015), the Terskey Ala Tau (Kutuzov and Shahgedanova, 2009), and the Zailiysky Alatau

* Corresponding author. Geomorphology and Glaciology, Department of Physical Geography, Stockholm University, Stockholm, Sweden.
E-mail address: robin.blomdin@natgeo.su.se (R. Blomdin).

http://dx.doi.org/10.1016/j.quascirev.2016.07.029
0277-3791/

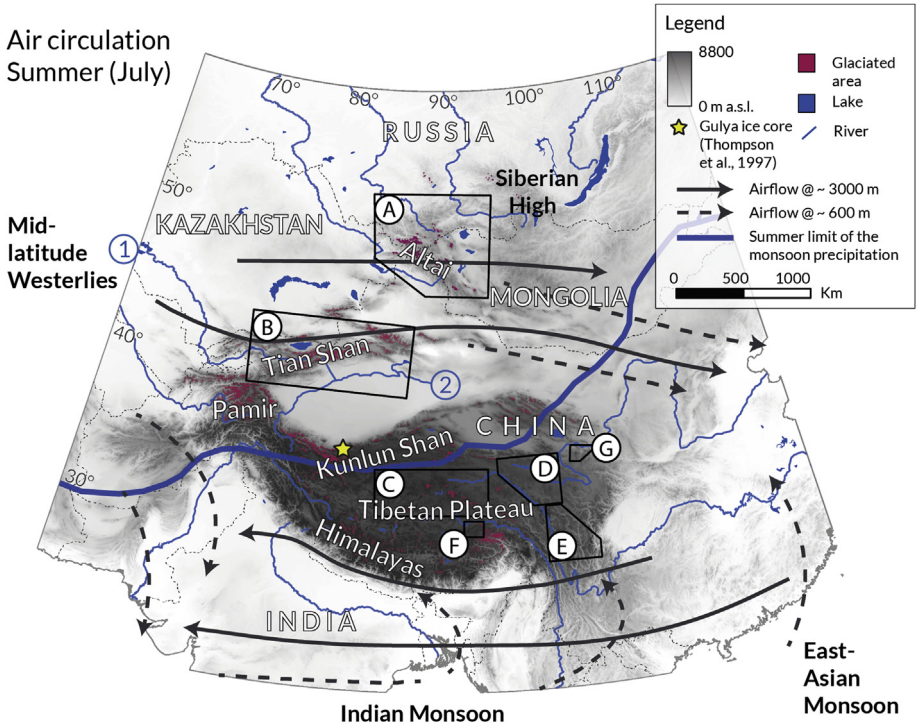

Fig. 1. Climatic setting and topographic features of Central Asia and the Tibetan Plateau. Location of glacial geomorphological maps produced for the region are indicated with black boxes and letters: A) Altai and western Sayan Mountains (Blomdin et al., 2016), B) Tian Shan (Stroeven et al., 2013), C) Tangula Shan (Morén et al., 2011), D) Bayan Har Shan (Heyman et al., 2008), E) Shaluli Shan (Fu et al., 2012), F) Maidika region (Lindholm and Heyman, 2015), and G) Dalijia Shan (Kassab et al., 2013). Also shown are the schematic locations and directions of air masses for the region (adapted after Benn and Owen, 1998 and Xu et al., 2010) and the northern present limit of summer monsoon precipitation (Shi, 2002). Numbers 1 and 2 indicate location of the Syr Darya and Tarim rivers, respectively. The yellow star refers to the location of the Guliya Ice Cap (Thompson et al., 1997). (For interpretation of the references to colour in this figure legend, the reader is referred to the web version of this article.)

(Bolch, 2007) ranges (Fig. 2). These studies indicate contrasting spatial variation in the response of glaciers to changes in climate. Glacier shrinkage has been less severe in the most continental ranges (e.g., the Ak-Shyirak Massif) and more severe in the more humid peripheral ranges to the north (e.g., the Kyrgyz Front Range and the Terskey Ala Tau Range; Sorg et al., 2012). In the early 21st century, the shrinkage rate of Ak-Shyirak glaciers has increased rapidly and they now suffer from mass losses similar to the northern ranges (Petrakov et al., 2016). This spatial variability in glacier shrinkage can be attributed to local environmental controls (elevation, aspect, latitude), affecting average temperature and incoming solar radiation (Farinotti et al., 2015). There are also links between the spatial variability of glacier shrinkage and large-scale climate dynamics. The Tian Shan is located at the confluence of several climate systems, including the mid-latitude Westerlies, the Siberian High pressure system, and both the Indian (South Asian) and East-Asian monsoons (Fig. 1). The mid-latitude Westerlies dominate the modern climate of the Tian Shan as the main source of precipitation, while the Siberian High pressure system further to the north brings cold winter temperatures to the region (Cheng et al., 2012). Glacial expansions or retreats are accordingly linked to the spatial variability in temperature and precipitation anomalies imposed by these climate systems as well as the local topographic context of the glaciated catchment.

A detailed understanding of past glacial episodes is an essential element in characterizing the impact of future climate changes in glaciated areas. We are focussing on glaciations across the Tian Shan and Central Asia, which has recently been the focus of many studies (Zhao et al., 2006, 2009, 2010, 2015; Narama et al., 2007, 2009; Koppes et al., 2008; Kong et al., 2009; Li et al., 2011, 2014; Zech, 2012; Lifton et al., 2014a). The fundamental motivation for most of these studies has been to present glacial chronologies, regional and hemispheric correlations, and to discuss possible paleoclimatic trends and mechanisms behind observed glacier expansions and recessions. Since glacier mass balance is coupled to climate, it has been recognised that robust glacial chronologies along west–east and north–south transects may enable reconstructions of past changes in atmospheric circulation (Koppes et al., 2008; Xu et al., 2010; Zech, 2012), allowing us to decipher the importance of different climate systems as drivers for past glaciation (cf. Dortch et al., 2013).

Comparison of glacial events across the Tian Shan requires the correlation of glacial chronologies across large regions. Obtaining these chronologies is a complex task (Barr and Clark, 2011), and issues include the nature of moraine formation, the accuracy of the ages, and correct interpretation of these ages. Marginal moraines are deposited along glacier snouts and have traditionally been interpreted to reflect ice margin positions during climatically stable periods (Benn and Evans, 2010). However, recent studies have indicated that the link between moraine formation and paleoclimate is not necessarily direct (Tovar et al., 2008; Reznichenko et al., 2011, 2012; Menounos et al., 2013; Gribenski et al., 2016). One important non-climatic driver behind moraine deposition is topographic control, so paleoclimatic inferences should only be drawn if this effect is absent or limited (Barr and Clark, 2012a; Barr and Lovell, 2014). Connecting moraine sequences between different valley systems is also complicated, and it is best to consider moraines with similar morphology (e.g., boulder concentration, volume/size, weathering, and vegetation cover; Kirkbride and Winkler, 2012). The availability of high-resolution remote-sensing imagery and digital elevation data, for systematic mapping of glacial footprints, has enhanced our ability to detect and map

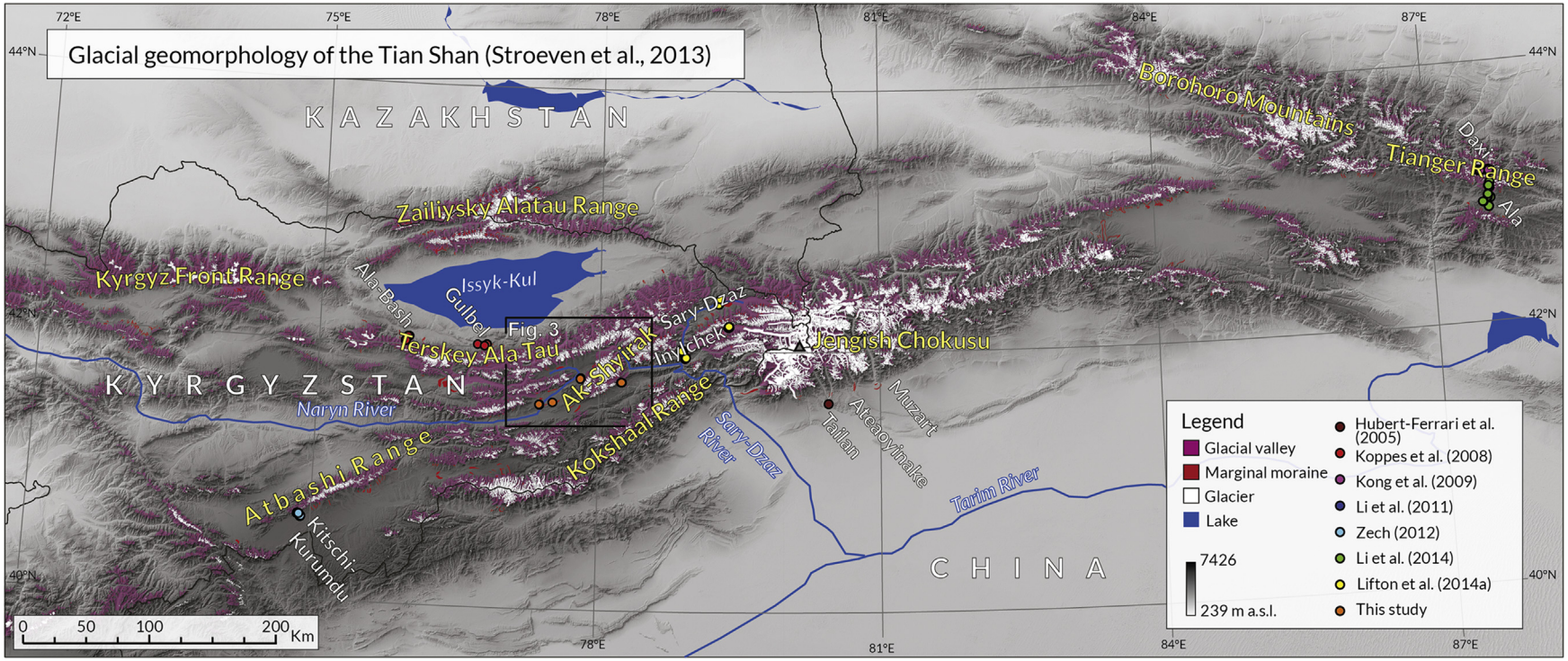

Fig. 2. Glacial geomorphology of the Tian Shan (Stroeven et al., 2013; B in Fig. 1). Also indicated is the location of the Ak-Shyirak map in Fig. 3 (black unfilled box). Colour-coded circles mark the locations of previous studies applying ^{10}Be exposure dating of glacial boulders on top of moraines. (For interpretation of the references to colour in this figure legend, the reader is referred to the web version of this article.)

moraines in formerly glaciated terrains (Glasser and Jansson, 2008; Heyman et al., 2008; Lovell et al., 2011; Barr and Clark, 2012b; Fredin et al., 2012; Blomdin et al., 2016; Darvill et al., 2014). This allows us to target suitable valleys for field investigations.

Surface exposure age dating using *in situ* cosmogenic nuclides is the primary means of dating when moraine boulders were deposited at the culmination of a glacier advance (e.g., Phillips et al., 1986, 1990; Nishiizumi et al., 1989; Briner et al., 2005; Owen et al., 2005; Schaefer et al., 2009; Kaplan et al., 2010; Jomelli et al., 2011). Our ability to identify and date moraines has increased dramatically over the past years, and several studies have attempted to move towards objective approaches of correlating glacial chronologies across regions (Dortch et al., 2013; Owen and Dortch, 2014; Murari et al., 2014) and hemispheres (Clark et al., 2009; Shakun et al., 2015). Given the strong need to develop a systematic and objective approach towards the correlation of dated moraines using cosmogenic dating, we specifically direct our attention to evaluating deglaciation age-accuracy and correlation robustness using new and previously published data from the Tian Shan in Central Asia.

2. Objectives and approach

This study aims to evaluate the timing of glacier expansion from suites of cosmogenic ages from moraines across the Tian Shan and to introduce a systematic approach to correlate glacial chronologies over a range of spatial scales (between valleys, and across mountain ranges and systems). The glacial history of the Tian Shan and the Ak-Shyirak area in central Kyrgyzstan, provide two case studies. For the Ak-Shyrak area we present new glacial geomorphological mapping and 25 new *in situ* ^{10}Be surface exposure ages from 6 moraines in an attempt to constrain the local timing of past glaciation. We also recalculate 89 previously published ^{10}Be surface exposure ages from 19 moraines (only considering moraines with $n \geq 3$ ^{10}Be exposure ages) across the Tian Shan. Thereafter we perform boulder erosion sensitivity tests and design a set of robustness criteria for moraine-specific boulder exposure age distributions, using simple statistics to characterise scatter and rejection of outliers. Moraine boulder distributions are assigned to one of three quality classes. Additionally we estimate the glacier altitudes and lengths for chronologically constrained moraines and finally we assign one of two significance tags to derived glacial stages *regional* or *local* depending on their individual and collective robustness and resolution and speculate on the degree to which one can make paleoclimate inferences from the available geochronological data.

3. Case studies: Tian Shan and the Ak-Shyirak area

3.1. Physical setting

The Tian Shan is a vast ~1200 km long WSW–ENE trending mountain belt straddling the borders of northwestern China, Kazakhstan, and Kyrgyzstan. The Tian Shan contains some of the highest peaks in the world outside of the Himalaya (Figs. 1 and 2). The mountain system was first uplifted during the Late Miocene (~8 million years ago) in response to the Tibetan Plateau reaching its maximum elevation (Abdrakhmatov et al., 1996). The region is an actively deforming intracontinental orogen, which formed in response to the continental collision between proto-India and proto-Asia (Molnar and Tapponnier, 1975; Zubovich et al., 2010). Several ranges exist throughout the region, bounded by reverse faults and separated by intermontane basins (Yin, 2010); deformation is accommodated by slip along numerous faults.

The Tian Shan acts as an effective barrier for moisture arriving with the mid-latitude Westerlies (Fig. 1). This results in relatively moist western (e.g., Kyrgyz Front Ranges) and northern ranges (e.g., Zailiysky Alatau Range; Fig. 2), continental eastern (e.g., Borohoro and Tianger Ranges; Fig. 2) and central ranges (Ak-Shyirak and Kokshaal Ranges; Sorg et al., 2012; Fig. 2), and dry southern ranges in northwestern China (Aizen et al., 1996). The timing of maximum precipitation varies across the region: the spring and early summer receive the most in the eastern and northern ranges; the late winter and early spring are the wettest in the western ranges; and the summer is wettest in the inner ranges (Sorg et al., 2012). This pattern reflects altitude; the high elevation sectors of the Tian Shan receive the highest precipitation totals later in the year. Annual precipitation decreases southward from 1000 mm north of the Kyrgyz Front Range to about 300 mm in the Ak-Shyirak area in the inner Tian Shan, and to less than 150 mm/year on the south slopes of the Tian Shan in China (Dyurgerov and Mikhalenko, 1995). Fig. 1 shows the location of Central Asia and the present-day limits of different climate systems (Owen et al., 2005; Shi, 2002). The present-day Indian- and East- Asian monsoons do not penetrate further north than the south slopes of the Kunlun Shan and eastern Mongolia, respectively (Fig. 1).

The Ak-Shyirak Massif is the second largest glaciated massif in the Kyrgyz sector of the Tian Shan and is located in the central part of the range (Figs. 2 and 3). The massif contains 193 glaciers covering an area of ~350 km^2 (Pieczonka and Bolch, 2015; Petrakov et al., 2016). Glaciers of the Ak-Shyirak Massif feed several of Central Asia's largest rivers, including the headwater of the Syr Darya, the Naryn River, which drains westward towards the Aral Sea region, and the Sary-Dzaz River, which is a tributary to the Tarim River and flows southward into northwestern China (Figs. 1 and 2). These glaciers and rivers are important for the region as they provide water security for millions of people in the densely populated downstream areas of Central Asia (Sorg et al., 2012; Farinotti et al., 2015).

3.2. Previous chronological work

Geochronological studies across the globe have allowed for the dating of ice limits for both glaciers and paleo ice sheets. The global last glacial maximum (gLGM) is a time period broadly defined by global ice volume and refered to as the marine oxygen isotope stage (MIS) 2 (14–29 ka; Lisiecki and Raymo, 2005). Results from several geochronological studies show that Northern Hemisphere glaciers and ice sheets were at their respective local last glacial maximum (lLGM) positions between 19 and 26.5 ka (Clark et al., 2009). Conversely, in the Tian Shan and in wider Central Asia and Tibet, a growing geochronological dataset is beginning to shed light on a contrasting story. While paleo-ice sheets on the Eurasian continent had a late maximum during the last glacial cycle (e.g., Stroeven et al., 2016), many paleoglaciers in Tibet and Central Asia reached their maximum extents earlier in the Pleistocene (Owen, 2013; Owen and Dortch, 2014). It is unclear whether these observations reflect an erosion-glacier length feedback mechanism (Kaplan et al., 2009; Anderson et al., 2012), are linked to changes in topography and moisture routing (Krinner et al., 2011), or require some other mechanism.

Narama et al. (2007, 2009) published the first absolute ages of the western Kyrgyz Tian Shan that we are aware of, using optically stimulated luminescence (OSL) dating on glacial till and loess covering marginal moraines. Their data indicated glacial expansions in the Atbashi Range (Fig. 2) between 18 and 33 ka. The timing of these glacial advances coincides with advances in the Terskey Ala Tau Range, however, here a more extensive glacial advance was dated to between 56 and 76 ka (Narama et al., 2009, Fig. 2). Koppes et al. (2008) further expanded on the glacial chronology of the

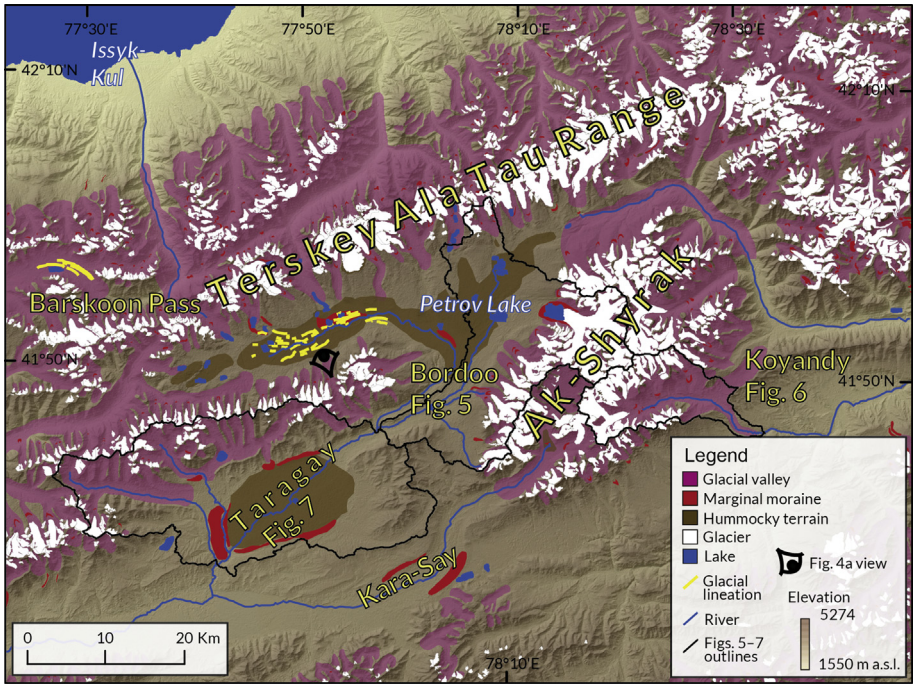

Fig. 3. Glacial geomorphology of the Ak-Shyirak area in the central Kyrgyz Tian Shan (Stroeven et al., 2013). Location of map is shown in Fig. 2. Also shown is Fig. 4a view and Fig. 5–7 outlines. (For the figure in colour, the reader is referred to the web version of this article.)

Kyrgyz Tian Shan with the first ^{10}Be surface exposure ages from the Atbashi, Terskey Ala Tau, and the Kyrgyz Front ranges (Fig. 2). Koppes et al. (2008) claimed glaciers reached their maximum positions in the northern and eastern Kyrgyz Tian Shan between 71 and 150 ka, during MIS 5 (71–130 ka; Lisiecki and Raymo, 2005) and MIS 6 (130–190 ka; Lisiecki and Raymo, 2005) and again between 57 and 71 ka, during MIS 4 (57–71 ka; Lisiecki and Raymo, 2005). The glacial history of the western Tian Shan was further expanded by Zech (2012), who dated three moraines on the southeast slopes of the Atbashi Range to ~15 ka (late MIS 2), ~21 ka (peak MIS 2) and >57 ka (MIS 4). Most recently, Lifton et al. (2014a) published a dual-isotope (^{10}Be, ^{26}Al) cosmogenic exposure chronology for moraines in the Inylchek and Sary-Dzaz valleys, valleys that emanate from the highest massif of the Tian Shan, the Jengish Chokusu Massif (Fig. 2). Their ^{10}Be exposure ages show evidence of advances by Inylchek Glacier at 15.6 ± 0.5 ka (late MIS 2), 22.4 ± 2.1 ka (peak MIS 2), between 71 and 80 ka, during MIS 4 or MIS 5, and potentially >160 ka during MIS 6. Data from the Sary-Dzaz valley show evidence of glaciers expanding between 22 and 30 ka (MIS 2).

Glacial geological work in the eastern Chinese Tian Shan has largely been concentrated around the Tian Shan Glaciological Station in the Daxi Valley on the northern slope of the Tianger Range (Fig. 2). The glacial record in this valley contains a sequence of five different tills (Zhao et al., 2006; Li et al., 2011). Several studies have tried to constrain the timing of glacier expansion using radiocarbon (Yi et al., 2004), electron spin resonance (ESR) (Yi et al., 2002; Zhao et al., 2006), and ^{10}Be surface exposure dating (Kong et al., 2009; Li et al., 2011, 2014). The three methods yielded very different age results, which has generated a discussion around both the interpretation of different deposits and the implication and meaning of the different dating techniques (Xu et al., 2010). Based on ^{10}Be surface exposure ages from previously unmapped moraines in Ala Valley on the southern slope of the Tianger Range (Fig. 2) and new and re-calculated ^{10}Be surface exposure ages in Daxi Valley, Li et al. (2014), concluded that major glacial advances occurred at ~25 ka (early MIS 2), between 37 and 50 ka, during MIS 3 (29–57 ka; Lisiecki and Raymo, 2005), between 50 and 80 ka (MIS 4), and at ~130 ka (MIS 6). The oldest glacial events are only recorded on the southern slope of the Tianger Range, and Li et al. (2014) attribute this to possible differences in microclimate and preservation potential.

The surface exposure ages of Li et al. (2014) from Daxi Valley are consistently younger than ESR ages from the same area (Yi et al., 2002; Zhao et al., 2006). This is important because it strengthens an emerging picture that ESR consistently provides older age estimates than other dating methods (Xu et al., 2010; Fu et al., 2013). A striking example relates to several large lateral moraines and piedmont moraine complexes on the south slopes of the Jengish Chokusu Massif (Fig. 2), below the mouths of the Ateaoyinake, Muzart, and Tailan valleys (Zhao et al., 2009, 2010, 2015). The moraines in these studies have been dated by ESR and provide evidence of the most extensive glacial advances occurring during MIS 11 or 12 in the Ateaoyinake Valley (Zhao et al., 2009), and during MIS 7 and 6 in the nearby Muzart and Tailan valleys (Zhao et al., 2010, 2015). Hubert-Ferrari et al. (2005), in a study on the deformation of faults, used ^{10}Be surface exposure dating of glacial boulders on the outermost set of piedmont moraines in the Tailan Valley and obtained late glacial ages. Similarly, a till of a marginal moraine dated by Zhao et al. (2015) as ~92 ka using ESR, was found to have a ^{10}Be exposure age of ~16 ka by Hubert-Ferrari et al. (2005).

4. Methods

4.1. Glacial geomorphological mapping

The regional glacial geomorphological map of the Tian Shan (Stroeven et al., 2013) forms a basis for high-resolution mapping, enables the selection of suitable sites for field investigations, and provides the context for ^{10}Be surface exposure age dating. We remap the area centred on the Ak-Shyirak Massif following a predefined set of criteria (Heyman et al., 2008; Stroeven et al., 2013).

The new mapping is based on the ASTER GDEM2 digital elevation model (Version 2 of the Advanced Spaceborne Thermal Emission and Reflection Radiometer Global Digital Elevation Model, http://www.gdem.aster.ersdac.or.jp), Landsat 7 satellite imagery (ETM+), and Google Earth imagery. The mapping utilises a GIS environment using on-screen manual digitising of glacial landforms. The map by Stroeven et al. (2013; Fig. 2) used the Shuttle Radar Topographic Mission (SRTM) DEM with a resolution of 3 arc-seconds (~90 m), while the ASTER GDEM2 has a resolution of 1 arc-second (~30 m). Although a comparison of the two techniques is not the emphasis of this work, we note some differences. The new map contains more mapped marginal moraines in the Bordoo and Koyandy valleys and in the Taragay Basin (Fig. 3). Other studies with the objective of comparing landform patterns and density using different resolution datasets also report a positive correlation between moderate to high resolution DEMs and number of moraines mapped (Barr and Clark, 2009, 2012b).

4.2. In situ ^{10}Be surface exposure dating

To determine the timing of glaciation across the Tian Shan we first compile 86 previously published ^{10}Be surface exposure ages, sampled on the crests of marginal moraines. We add to this dataset 25 new ^{10}Be exposure ages, from two valleys of the Ak-Shyirak Massif with opposing west–east aspects: the Bordoo and Koyandy valleys (Fig. 3), and a large moraine complex in an intermontane basin southwest of the Ak-Shyirak Massif – the Taragay moraine complex (Fig. 3). Quartz-rich rock samples were collected in 2012 using chisel and hammer from the top surfaces of glacial boulders (preferably >1 × 1 × 1 m) located on either lateral- or frontal moraine crests (Sample contextual information is provided in Table 1 and the supplementary dataset).

Physical preparation and chemical treatment of the rock samples were performed at PRIME Lab, Purdue University. Mineral separation and isolation of quartz followed a protocol based on the standard procedures developed by Kohl and Nishiizumi (1992), and purity of the quartz was checked by measuring the Al content of the samples using Inductively Coupled Plasma – Optical Emission Spectrometry (ICP-OES). Clean quartz samples were then spiked with a Be carrier (concentration: 1069±8 ppm μg/g) and dissolved. Beryllium was then isolated using standard ion exchange chromatography (Strelow et al., 1972; Ochs and Ivy-Ochs, 1997) and oxidized. Finally, the ^{10}Be/^{9}Be ratios were measured at PRIME Lab using accelerator mass spectrometry (AMS), with normalization using the ^{10}Be standards prepared by Nishiizumi et al. (2007) with a value of 2.85×10^{-12}, using the ^{10}Be half-life of 1.36×10^{6} years. The ratios were converted to ^{10}Be concentrations using sample weights and total beryllium (Balco, 2006; Table 1 and the supplementary dataset).

4.3. Surface exposure age calculations

We calculate zero-erosion exposure ages using the CRONUS online calculator code (Balco et al., 2008; http://hess.ess.washington.edu), modified with ^{10}Be production based on the nuclide-specific LSD spallation and muon production rate scaling of Lifton et al. (2014b) and the muon production parameterization of Phillips et al. (2016) (Heyman et al., 2016). In the calculation, corrections for topographic shielding were included; corrections for vegetation and snow cover were omitted because we do not have any estimates on the effect of vegetation and snow cover on cosmogenic production in these areas. Accurate determination of an exposure age relies furthermore on how well we can estimate the cosmogenic nuclide production rate and boulder surface erosion rates. Over the years numerous independently dated calibration sites have been established to determine reference production rates, and different scaling schemes have been developed to describe how cosmogenic production rates vary across space and time. Using a statistical fitting exercise Borchers et al. (2016) demonstrated discrepancies between different scaling frameworks. For example the scaling frameworks based on neutron monitors (e.g. Dunai, 2001; Desilets and Zreda, 2003; Lifton et al., 2005; Desilets et al., 2006) have inferior fits to calibration datasets relative to scaling schemes based on measurements of atmospheric nuclear disintegrations and neutron detectors covering a range of energies, both with and without paleomagnetic corrections (Nishiizumi et al., 1989; Lal, 1991; Stone, 2000). Negligible differences in performance were observed between the older scaling schemes (Nishiizumi et al., 1989; Lal, 1991; Stone, 2000; Balco et al., 2008) and the more recent LSD scaling framework, based on simulated cosmic-ray fluxes (Lifton et al., 2014b), obtaining best-fitting ^{10}Be production rates ranging between 3.9 and 4.1 atoms g^{-1} yr^{-1}. We choose the LSD model over previous ones because it predicts scaling behaviour more consistently at high-altitudes and low-latitude locations (Lifton et al., 2014b).

Since there are no production rate calibration sites from Central Asia (Blard, 2016), we have to rely on a global ^{10}Be spallation reference production rate. Global rates have previously been calculated, using nuclide-specific LSD scaling (e.g., Shakun et al., 2015; Borchers et al., 2016; Heyman et al., 2016; Lifton, 2016; Phillips et al., 2016). These studies differ in their approach regarding fitting, averaging of data, and number of sites included in the dataset but agree within their uncertainties. We adopt a ^{10}Be spallation reference production rate of 3.98 ± 0.17 atoms g^{-1} yr^{-1}, based on 22 well-clustered ^{10}Be production rates (Heyman et al., 2016). This reference production agrees (within errors) with those of Shakun et al. (4.0 ± 0.1 atoms g^{-1} yr^{-1}) and Borchers et al./Phillips et al. (3.92 ± 0.31 atoms g^{-1} yr^{-1}). For our study area, the uncertainties related to latitude scaling are likely minimal, since the calibration sites cover a range of different latitudes, although there might be additional uncertainties involved in altitude scaling, since our study area is on average > 2500 m a.s.l. and most calibration sites are located closer to sea level (cf. Lifton et al., 2014a). However, whilst production rate and scaling schemes are important, over a relatively small geographic area/altitude it is unlikely to make as much of a difference as geomorphic uncertainty.

Because exposure ages in this study were derived assuming zero post-glacial erosion of the boulder surface and neglect the effect of shielding by snow and vegetation, our calculated ages are considered to be minimum exposure ages. The zero-erosion assumption is based on our sampling strategy to target stable varnished surfaces on glacial erratics (cf. Lifton et al., 2014a). However, we also investigate the effect of including boulder erosion rates of 1, 3, and 5 mm kyr^{-1} on exposure ages. The 1 and 3 mm kyr^{-1} estimates have been used previously to calculate minimum and maximum exposure ages in Kyrgyzstan (Koppes et al., 2008). The zero-erosion exposure age of an eroded surface will always be less than an exposure age including erosion correction because the sampled rock surface has been partially shielded from cosmic rays (Balco, 2011).

4.4. Surface exposure age data analysis

We assess the robustness of individual boulder groups and compare the new Ak-Shyirak exposure ages with previous exposure age studies from the Tian Shan (Hubert-Ferrari et al., 2005; Koppes et al., 2008; Kong et al., 2009; Li et al., 2011, 2014; Zech, 2012; Lifton et al., 2014a). We also assign discrete glacial stages to moraines and distinguish whether these glacial stages are of local or regional significance (cf. Dortch et al., 2013). We then adopt an

Table 1
Sample information and ^{10}Be results from the Ak-Shyirak area.

ID	Group ID	Lat	Long	Altitude	Sample depth	Topo shielding	^{10}Be	±(Atoms g^{-1})	LSD age	Ext ±	Int ±
		°	°	(m a.s.l.)	(cm)		(Atoms g^{-1})		(ka)	(ka)	(ka)
TS-C-12-007	TAR 2	41.6189	77.7290	3422	1.5	1.00	3,547,186	55,672	69.8	3.2	1.1
TS-C-12-008	TAR 2	41.6192	77.7288	3419	4.0	1.00	4,196,385	69,487	85.0	4.0	1.4
TS-C-12-009	TAR 2	41.6219	77.7262	3426	1.0	1.00	3,819,334	67,242	74.7	3.5	1.3
TS-C-12-010	TAR 2	41.6221	77.7261	3428	3.0	1.00	4,092,253	65,712	81.6	3.8	1.3
TS-C-12-011	TAR 2	41.6223	77.7213	3418	2.0	1.00	2,474,425	41,992	48.8	2.3	0.8
TS-C-12-035	TAR 1	41.6430	77.8641	3509	2.5	1.00	1,445,967	29,763	28.3	1.3	0.6
TS-C-12-036	TAR 1	41.6433	77.8649	3508	3.0	1.00	950,020	19,401	19.5	0.9	0.4
TS-C-12-037	TAR 1	41.6403	77.8500	3501	2.0	1.00	2,081,114	30,525	39.4	1.8	0.6
TS-C-12-019	BOR 3	41.8166	78.1171	3791	2.0	0.99	1,149,114	51,980	19.6	1.2	0.9
TS-C-12-020	BOR 3	41.8168	78.1169	3790	4.5	1.00	1,433,923	43,784	24.3	1.3	0.7
TS-C-12-021	BOR 3	41.8171	78.1143	3762	1.0	1.00	681,262	26,772	12.3	0.7	0.5
TS-C-12-022	BOR 3	41.8171	78.1148	3762	3.0	1.00	935,566	28,253	16.7	0.9	0.5
TS-C-12-023	BOR 2	41.8158	78.1151	3734	4.0	0.99	747,864	25,921	14.0	0.8	0.5
TS-C-12-025	BOR 2	41.8144	78.1118	3706	3.0	0.99	580,511	15,413	11.1	0.6	0.3
TS-C-12-026	BOR 2	41.8143	78.1118	3706	1.0	1.00	847,942	13,672	15.5	0.7	0.3
TS-C-12-027	BOR 1	41.8125	78.1319	3775	2.0	0.99	25,155	3735	0.6	0.1	0.1
TS-C-12-028	BOR 1	41.8124	78.1314	3776	2.0	0.99	289,587	12,583	5.4	0.3	0.2
TS-C-12-029	BOR 1	41.8121	78.1299	3759	2.5	0.99	172,311	10,105	3.3	0.2	0.2
TS-C-12-030	BOR 1	41.8122	78.1301	3766	2.6	0.99	31,584	4217	0.7	0.1	0.1
TS-C-12-031	BOR 1	41.8124	78.1305	3769	2.0	0.98	49,461	2187	1.1	0.1	0.0
TS-C-12-046	KOY 1	41.7902	78.5058	3412	1.5	0.99	528,617	11,417	11.9	0.6	0.3
TS-C-12-047	KOY 1	41.7903	78.5040	3424	1.5	0.990	731,527	15,183	16.0	0.8	0.3
TS-C-12-048	KOY1	41.7905	78.5037	3430	3.0	0.99	436,426	10,484	10.0	0.5	0.2
TS-C-12-049	KOY 1	41.7898	78.5000	3442	2.5	0.97	752,688	18,077	16.7	0.8	0.4
TS-C-12-050	KOY 1	41.7894	78.5004	3441	2.5	0.98	763,717	16,059	16.8	0.8	0.4

Notes: ^{10}Be was converted from measured ^{10}Be/^{9}Be ratios at PRIME Lab, Purdue University, using accelerator mass spectrometry (AMS) with normalization using the ^{10}Be standards prepared by Nishiizumi et al. (2007) with a value of 2.85×10^{-12}, using the ^{10}Be half-life of 1.36×10^{6} years. Six different blank samples were used for background correction.

- Samples TS-C-12-007, 9, 10 with blank of 196,047 ± 48,161 at g^{-1} carrier (0.2495 g, 1069 ppm Be, $11.0 \pm 2.7 \times 10^{-15}$ ^{10}Be/^{9}Be).
- Samples TS-C-12-008, 27–30, with blank of 166,925 ± 23,085 at g^{-1} carrier (0.2686 g, 1069 ppm Be, $8.7 \pm 1.2 \times 10^{-15}$ ^{10}Be/^{9}Be).
- Samples TS-C-12-023, 25, 26, 31 with blank of 62,764 ± 13,464 at g^{-1} carrier (0.2092 g, 1069 ppm Be, $4.2 \pm 0.9 \times 10^{-15}$ ^{10}Be/^{9}Be).
- samples TS-C-12-019-22 with blank of 155,259 ± 51,776 at g^{-1} carrier (0.2415 g, 1069 ppm Be, $9.0 \pm 3.0 \times 10^{-15}$ ^{10}Be/^{9}Be).
- Samples TS-C-12-046-50 with blank of 45,835 ± 13,248 at g^{-1} carrier (0.2467 g, 1069 ppm Be, $2.6 \pm 0.8 \times 10^{-15}$ ^{10}Be/^{9}Be).
- Samples TS-C-12-011, 35–37 with blank of 114,922 ± 34,718 at g^{-1} carrier (0.2456 g, 1069 ppm Be, $6.6 \pm 2.0 \times 10^{-15}$ ^{10}Be/^{9}Be).

All ^{10}Be surface exposure ages have been calculated assuming no surface erosion implying that these are minimum ages. Rock density for sample thickness correction is assumed to be 2.65 g cm^{-3}. Ages are reported using the nuclide-specific LSD production rate scaling (Lifton et al., 2014b) and a global ^{10}Be spallation reference production rate of 3.98 ± 0.17 atoms g^{-1} yr^{-1} (Heyman et al., 2016). Internal uncertainties include error in blank, carrier mass, and counting statistics, while external errors also include production rate uncertainties.

approach modified from Heyman (2014) and assess the degree of age clustering of each group of samples from a particular moraine by separating well-clustered from moderately- and poorly-clustered exposure age groups. It is well-known that exposure age distributions on moraines often show significant scatter (cf. Hallet and Putkonen, 1994; Putkonen and Swanson, 2003; Briner et al., 2005; Applegate et al., 2010, 2012; Heyman et al., 2011). Two conditions are believed to potentially skew exposure age distributions of glacial boulders on moraines, masking their true age of deposition – cosmogenic inheritance through prior exposure (resulting in an overestimate of the exposure age) or incomplete exposure through post-depositional shielding and subsequent erosion (resulting in an exposure age underestimate). Since post-depositional shielding is commonly the dominant process, the oldest exposure age within a range of ages is often the best age to select as the minimum moraine depositional age when scatter is significant (Briner et al., 2005), which has also been indicated by Monte Carlo exposure age modelling by Heyman et al. (2011). Others have instead concluded that nuclide inheritance is more common than incomplete exposure and suggested that the youngest samples best estimated the true age of moraine formation (Benson et al., 2005) and there are occasions where the geomorphic context implies that inheritance is more likely (Darvill et al., 2015a).

4.4.1. Robustness criteria

We first adopt Peirce's Criterion (Peirce, 1852, 1877; Gould, 1855; Ross, 2003) to eliminate outliers from the dataset. When there is a concern that the arithmetic mean of a group of samples is not robust enough, Peirce's Criterion can be used to determine a threshold value for which outliers can be confidently rejected. Samples are rejected if their deviation from the sample mean is larger than the maximum allowable deviation, which is determined by multiplying the standard deviation of the sample with *R* ("the ratio of maximum allowable deviation from the data mean to the standard deviation"; Ross, 2003; supplementary dataset). In three additional cases we decided to go with the original authors and reject outliers based on their recommendation. These samples are: TS-IN-04, -06 and -08 (supplementary dataset) of Lifton et al. (2014a). The rejection of -04 and -08 is motivated by their low quartz yield of ~1% quartz resulting in poor counting statistics and wide error margins, while the rejection of -06 was recommended due to evident post-depositional effects (Lifton et al., 2014a). All individual exposure age uncertainties, when discussed, are reported with their external uncertainties (including errors in Be blank measurement, carrier mass uncertainty, AMS counting statistics, and production rate uncertainties).

Given the uncertainties regarding the interpretation of scattered datasets in terms of true age of moraine formation, when scatter is significant, we refrain from adopting extreme age estimators and present the mean ages of our respective sample groups for correlation of glacial events. Based on the approach advocated by Heyman (2014), we analyse the scatter of exposure ages for each

site/landform by designing a set of robustness criteria in order to categorize the sets of ages as belonging to one of three quality classes, A (well-clustered), B (moderately clustered) and C (poorly clustered). In this analysis we only consider boulder populations belonging to moraines with $n \geq 3$ exposure ages.

We first assume that the spread in exposure ages is normally distributed and that their uncertainties represent the dispersion in age, and calculate the reduced Chi-Square statistic (χ^2_R) using analytical (internal) uncertainties (Balco, 2011). This statistic is a measurement of excess scatter and it is a confirmation of whether the observed scatter can be expected from the measurement uncertainty alone. If the value of this statistic is close to one, the data is well described by a normal distribution, with scatter around the mean described by the measurement uncertainty (Balco, 2011). Whether this assumption is appropriate or not is debatable. For example, the CRONUS-Earth intercomparison recently found that there is some interlaboratory scatter in excess of measurement uncertainties (Jull et al., 2015). This would, however, only be an issue if different labs analysed boulders from the same moraine, which is never the case for our dataset. Furthermore, analysed sample groups range between populations of three to ten samples. It is important to note that χ^2_R is less robust for small sample populations and that the probability of getting low χ^2_R values increases with sample size. This does not impact our analysis, as we are simply classifying our data and not rejecting any data based on this statistic.

After rejecting outliers using Peirce's Criterion and computing χ^2_R (satisfying that $n \geq 3$) we assign sample groups to quality classes A, B or C (supplementary dataset):

1. **Class A** (well-clustered) exposure age groups have $\chi^2_R \leq 2$. In this case we report the arithmetic mean and standard deviation (1σ), assuming that this represents the deglaciation age of the moraine and that geomorphological processes have had little or no impact in causing deviation of the exposure ages from the true age of the landform.
2. **Class B** (moderately clustered) exposure age groups have $\chi^2_R > 2$ but a standard deviation $\leq$15% of the mean exposure age. In this case we report the arithmetic mean and standard deviation (1σ), assuming that this represents the deglaciation age of the moraine and that geomorphological processes have had some effect on the spread of exposure ages.
3. **Class C** (poorly-clustered) exposure age groups have large scatter ($\chi^2_R > 2$), and a standard deviation >15% of the mean exposure age. In this case we report the arithmetic mean and standard deviation (1σ), assuming that this represents the deglaciation age of the moraine and that geomorphological processes have had large impact on the spread of exposure ages.

For these quality classes the standard deviation (1σ) is believed to represent the deglaciation age uncertainty (Heyman, 2014). Unlike Heyman (2014) we do not include outliers in this calculation as we apply Peirce's Criterion to identify outlier exposure ages. We label boulder groups with a 3-letter code for location and a number reflecting relative age chronology (1 being youngest; e.g., BOR 1–BOR 3 for successively older boulder groups in the Bordoo Valley). After having performed this division into quality classes, we proceed to define the timing of local and regional glacial stages.

4.4.2. Glacial stage correlation

Our analysed boulder age groups are all from specific moraines, and we assume that these moraines reflect former stationary ice margin positions (Benn and Evans, 2010). Thus, boulder ages from a moraine should represent the timing of onset of deglaciation. As discussed above, several geomorphological processes affect boulder age distributions on moraines thereby partially obscuring deglaciation estimates. The timing of a (local) glacial stage is defined as the arithmetic mean and standard deviation (1σ) of the boulder age population. When the age ranges of two or more moraines overlap within their error bounds they define a regional stage. This approach yields a conservative estimate with wide error margins. For many boulder groups (especially class C), large error margins make it difficult to distinguish between potentially different populations. Hence, when analysing the regional significance of glacier expansion, we only consider quality class A and B boulder groups. The large scatter of class C exposure age groups prohibits their inclusion in a regional correlation.

4.5. Paleoglacial attributes

To allow for comparison of chronologically-constrained glacier limits across the Tian Shan we consider two different paleoglacial attributes. We estimate glacier lengths as the distance between the ice distal part of a mapped moraine and the headwall of the closest catchment from which the paleoglacier was likely sourced and glacier altitudes as the lowest elevation of mapped moraines in Google Earth. When estimating paleoglacial attributes from mapped moraines we only consider moraines with class A and B boulder groups.

5. Results

5.1. Glacial geomorphology

This result section summarises the mapping presented in Stroeven et al. (2013) and our new mapping for the Ak-Shyirak area. The glacial geomorphology of the Tian Shan contains a rich record of glacial landforms, with extensive sets of marginal moraines and glacially eroded valleys occurring in high elevation areas, while lower-lying terrain commonly lacks traces of glaciation. Large complexes of moraines have been mapped in the western Tian Shan on the south slopes of the Atbashi Range, on the southern slopes of the Jengish Chokusu Massif, and outside the southern mountain front of the Tianger Range (Fig. 2). Extensive marginal moraines have also been mapped on the northern slopes of the Terskey Ala Tau Range. Marginal moraines deposited beyond the mountain front likely formed along piedmont lobes as the geometry of such moraines often reflects this shape. The dimensions of the mapped moraines range between c. 0.2 km and 18 km in length and are <0.5 km in width.

The glacial geomorphology of the Ak-Shyirak area and the surrounding mountains and basins mirrors that of the Tian Shan at large except that glaciers here extended particularly far beyond the extent of mapped glacial valleys (Figs. 3 and 4). In addition to successions of moraines in glacial valleys indicative of restricted glacier advances (Figs. 5 and 6), this area has also abundant evidence for more extensive glacier extents. Streamlined ridges, for example, east of the Barskoon Pass, paralleling the axis of the main valley (Fig. 3), have been interpreted as glacial lineations (Stroeven et al., 2013); i.e. subglacial landforms formed parallel to former ice flow directions (Benn and Evans, 2010, Fig. 4a). Extensive successions of marginal moraines, hummocky terrain, and meltwater channels located in the Taragay Basin, are other landform examples for extensive glaciation (Figs. 3 and 7). Similarly, during our fieldwork in 2012 we found till and erratics on the interfluves in both the Bordoo and Koyundi valleys also indicating extensive glaciation.

5.2. Surface exposure ages

5.2.1. Tian Shan glacial chronology

The timing of paleoglaciation in the Tian Shan is difficult to

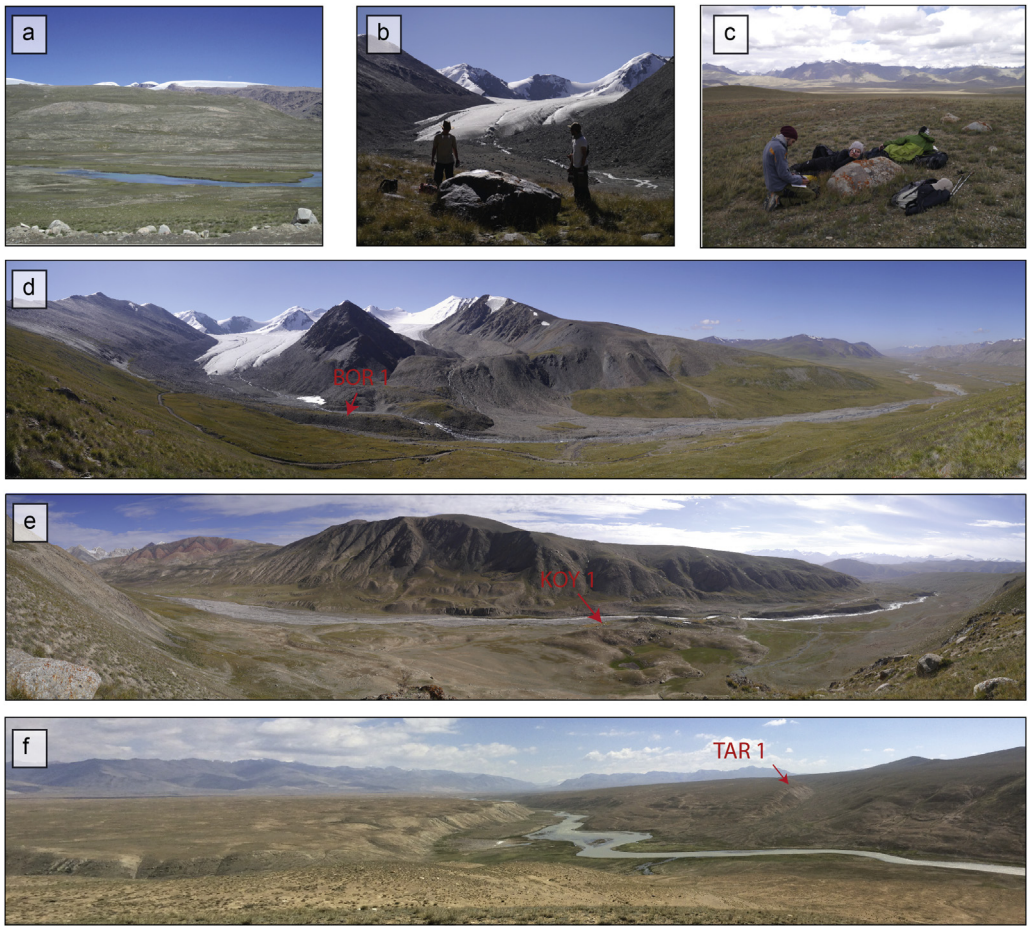

Fig. 4. Field photographs: a) Glacial lineations on the southern slopes of the Terskey Ala Tau Range (Barskoon Pass), b) Bordoo Valley: Sample TS-C-12-028 of glacial erratic located on the BOR 1 marginal moraine. c) Taragay moraine complex: Sample TS-C-12-007 of glacial erratic located on the TAR 2 moraine. d) Panorama of the upper Bordoo Valley showing the BOR 1 moraine. View towards south. e) Panorama of the lower Koyandy watershed. View towards the north and the KOY 1 marginal moraine. f) Panorama of the Taragay Basin. View towards northeast and the TAR 1 moraine. Taragay River draining to the south. See Figs. 3 and 5–7 for location of photographs a, d, e and f. (For photographs in colour, the reader is referred to the web version of this article.)

constrain due to large scatter in minimum surface exposure ages from moraines. However, combining the recalculated previously published data with our new data from the Ak-Shyirak area allows us to derive some consistent patterns. In general, the surface exposure ages scatter a lot for individual moraines and this scatter is especially pronounced for moraines that were deposited prior to MIS 2 (Fig. 8).

When we perform our quality test on the complete Tian Shan dataset, we find an acceptance of only three moraines as well-constrained (class A) with an average relative uncertainty of ~5%. Seven moraines are categorized as moderately constrained (class B) and have an average relative uncertainty of ~10%, the remaining boulder groups (n = 15) have an average relative uncertainty of ~38% (Fig. 8 and supplementary dataset). Hence, ~60% of the moraines have had an influence of geological processes, such as inheritance or post-depositional shielding, dominating the spread of ages. Nine ages were rejected using Peirce's Criterion or based on author recommendations (Lifton et al., 2014a dataset).

5.2.2. Ak-Shyirak glacial chronology

We collected 12 glacial boulders from three moraines for surface exposure dating in the **Bordoo Valley** (Fig. 5; BOR 1–3). The age scatter for 3–5 individual boulders on the same landforms is generally high. BOR 1 (Figs. 4d and 5) is located about 1 km down-valley from the contemporary glacier snout and has a stable vegetated surface. Five minimum exposure ages derived from boulders on this moraine range from 5.4 ± 0.3 to 0.6 ± 0.1 ka (Table 1 and Fig. 5). Peirce's Criterion allows the rejection of the oldest age but because χ^2_R remains ≥100 and the standard deviation is >15% of the mean exposure age, this group is assigned to class C quality with a mean age of 1.4 ± 1.3 ka (Fig. 8). Furthermore, three samples, with exposure ages of 11.1 ± 0.6, 14.0 ± 0.8 and 15.5 ± 0.7 ka (Table 1) were taken from boulders on a distinct marginal moraine ridge (BOR 2), ~1 km down-valley from BOR 1 (Fig. 5). These samples have a χ^2_R of ~70 and a standard deviation > 15% of the mean exposure age. This group is therefore classified as exhibiting exposure age class C quality and the deglaciation age for BOR 2 is 13.2 ± 2.2 ka (n = 3) (Fig. 8). Finally, four samples from BOR 3 (Figs. 4b and 5) yielded a deglaciation age of 18.2 ± 5.1 ka (n = 4). This group is also assigned an exposure age class C, because χ^2_R = ~80, and the standard deviation to mean exposure age ratio is >15% (Fig. 8).

Five samples collected from a terminal moraine located in the **Koyandy Valley** (KOY 1; Figs. 4e and 6), yielded minimum exposure ages ranging between 10.0 ± 0.5 and 16.8 ± 0.8 ka (Table 1). Peirce's Criterion would not allow rejection of potential outliers, so χ^2_R = ~140 and the standard deviation to mean exposure age ratio is >15%. We therefore assign this group an exposure age class C quality with a deglaciation age of 14.3 ± 3.1 ka (n = 5) (Fig. 8).

Finally, we collected eight samples from two distinctly different

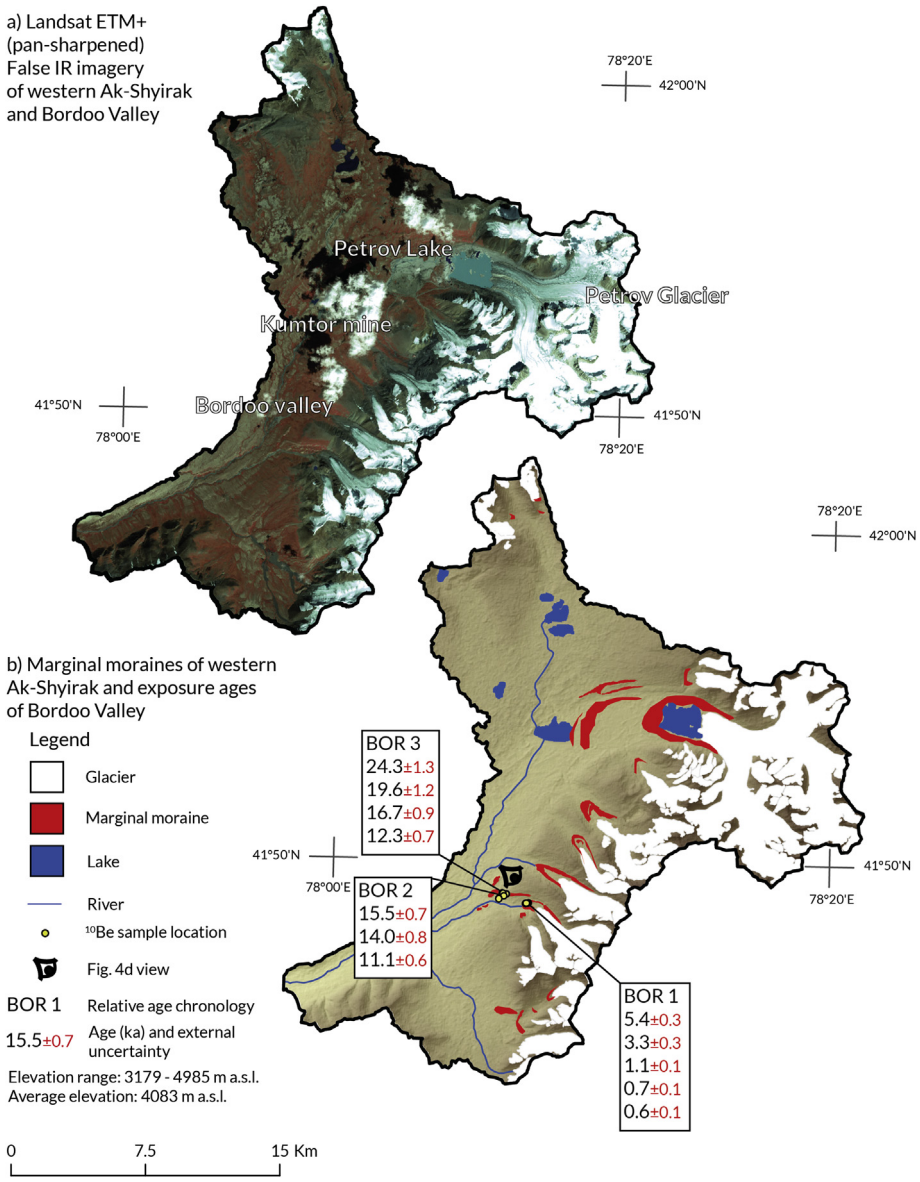

Fig. 5. a) Landsat ETM+ (pan-sharpened) False IR imagery of the western Ak-Shyirak watershed, including Bordoo Valley. b) Mapped marginal moraines and location of ^{10}Be samples with associated exposure ages (ka). Labels BOR 1 – BOR 3 reflect relative age chronology, 1 being youngest. Location of the figure outline is indicated in Fig. 3. Also shown is Fig. 4d view. (For the figure in colour, the reader is referred to the web version of this article.)

moraine ridges (TAR 1 and 2) that comprise the outer part of a large terminal moraine complex in the **Taragay Basin** (Figs. 4f and 7). The ages of three samples from TAR 1 (Fig. 4f) range from 19.5 ± 0.9 to 39.4 ± 1.8 ka (Table 1) and this age group therefore fails our exposure age classes A and B criteria and the deglaciation age of TAR 1 is 29.1 ± 10.0 ka (Fig. 8). Five samples from TAR 2 reveal an age range of 48.8 ± 2.3 to 85.0 ± 4.0 ka (Fig. 7). Peirce's Criterion allows for the rejection of the young outlier and after outlier rejection TAR 2 has a deglaciation age of 77.8 ± 6.8 ka (Class B; n = 4). This is the oldest moderately constrained maximum extent of glaciation recorded in the Ak-Shyirak study area (Fig. 8).

5.2.3. Boulder erosion sensitivity

Assessing the effect of postglacial erosion rates on derived exposure ages is difficult since there are, to our knowledge, no site-specific studies of erosion rates in the Tian Shan. Nevertheless, when investigating the effect of different rates of boulder erosion, the influence is generally negligible for younger ages (<25 ka), with an average age increase for high rates of erosion (5 mm kyr^{-1}) of ~5% in exposure age (Fig. 9). Between 25 and 50 ka, lower erosion rates (1 mm kyr^{-1}) have little effect on ages while higher rates have a significant effect with an average age increase of ~15% (Fig. 9). For samples older than 100 ka, erosion has a significant effect on exposure ages, with age changes ranging from 15% to 60% (Fig. 9). For older samples, uncertainties are large, especially in the face of unquantifiable post-depositional boulder surface erosion rates.

5.3. Glacier lengths and altitudes

Estimated glacier altitudes and lengths for paleoglaciers depositing moraines with chronological constraints (classes A and B) are presented in Table 2. For the western Tian Shan there are only two mapped and chronologically constrained moraines (KIT 1–2) from one site in Kitschi-Kurumdu. These paleoglaciers extended

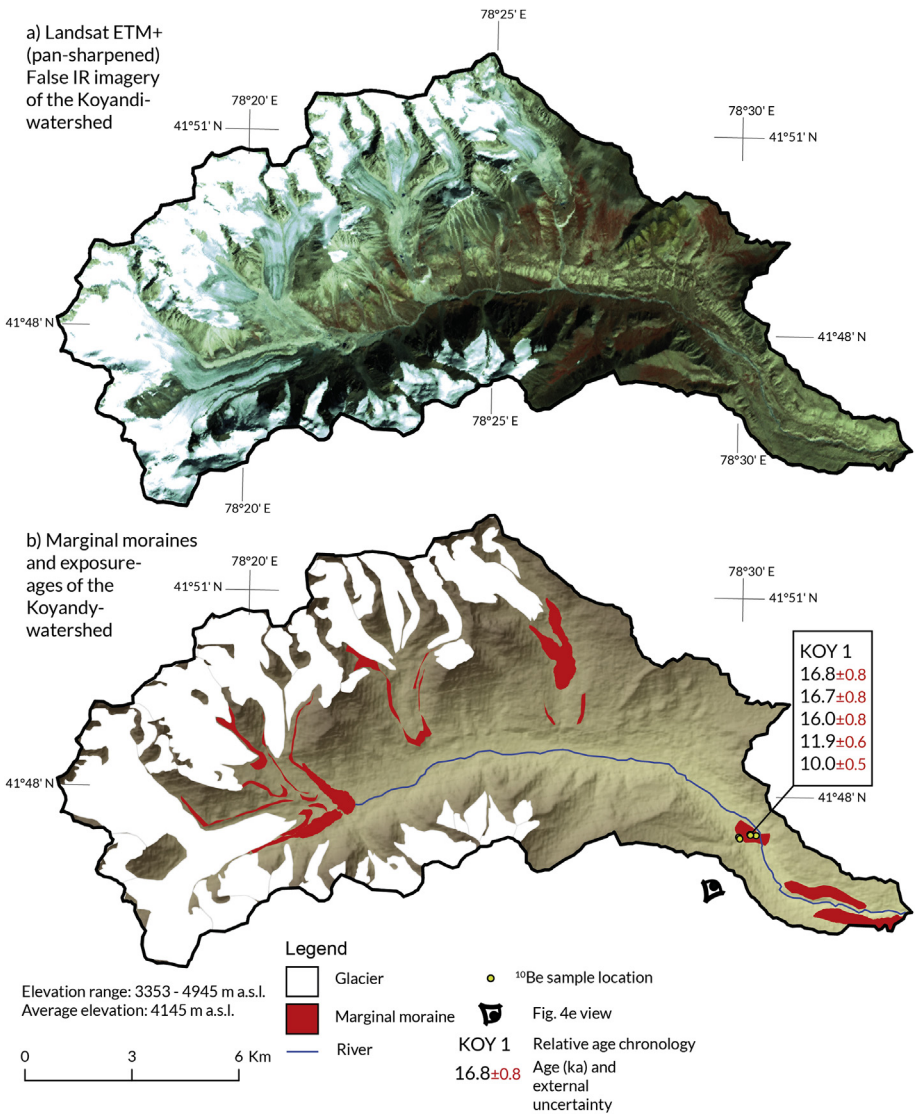

Fig. 6. a) Landsat ETM+ (pan-sharpened) False IR imagery of the Koyandy watershed. b) Mapped marginal moraines and location of ^{10}Be samples with associated exposure ages (ka). Label KOY 1 indicates relative age chronology, however only one moraine was sampled in Koyandy Valley. Location of the figure outline is indicated in Fig. 3. Also shown is Fig. 4e view. (For the figure in colour, the reader is referred to the web version of this article.)

down to altitudes of 3800 and 3700 m a.s.l. and were 3–4 km long, respectively. In the central parts of the Tian Shan glacier altitudes of four robustly dated moraines ranged between 2600 and 3400 m a.s.l. and glacier lengths ranged between 43 and 112 km. Finally in the eastern sector of the Tian Shan glacier altitudes of four robustly dated moraines ranged between 3100 and 3500 m a.s.l. while glacier lengths ranged between 1 and 15 km.

6. Discussion

6.1. Maximum extent of paleoglaciation

The maximum extent of glaciation in the Ak-Shyirak area is consistent with data provided by Stroeven et al. (2013). For numerous sites across the Tian Shan, glaciers seem to have extended beyond the confinement of individual valleys with spatial variability depending on the topographic context (Zhao et al., 2006, 2009, 2010, 2015; Narama et al., 2007, 2009; Koppes et al., 2008; Kong et al., 2009; Li et al., 2011, 2014; Lifton et al., 2014a). We recognise that future field investigators may locate till and erratics distal from mapped marginal moraines and that these observations may provide evidence for more extensive glaciations (cf. Heyman et al. (2009), who coined the term "minimum extent of maximum glaciation"). Nevertheless, remote-sensing-based data do not indicate glacial landform evidence consistent with large-scale (ice sheet) glaciations as proposed for this area by Grosswald et al. (1994) and Kuhle (2011). Evidence from cosmogenic nuclide dating indicates the presence of valley glaciers through different stages of the last glacial cycle, which additionally refutes the presence of an ice sheet during this time.

Glacial geomorphological evidence from the Ak-Shyirak area provides unambiguous proof of extensive paleoglaciers extending down into the intermontane basins (Figs. 3 and 5–7). The spatial distribution of marginal moraines, hummocky terrain, and glacial lineations in the areas surrounding the Ak-Shyirak Massif, indicates that valley glaciers merged to form large ice lobes, depositing extensive marginal moraines and mantling the interfluves with till. We conclude that the approximate glacier length (distance from terminal moraine to catchment headwall) of the paleoglacier depositing BOR 2 (~7 km), close to the mouth of Bordoo Valley, was

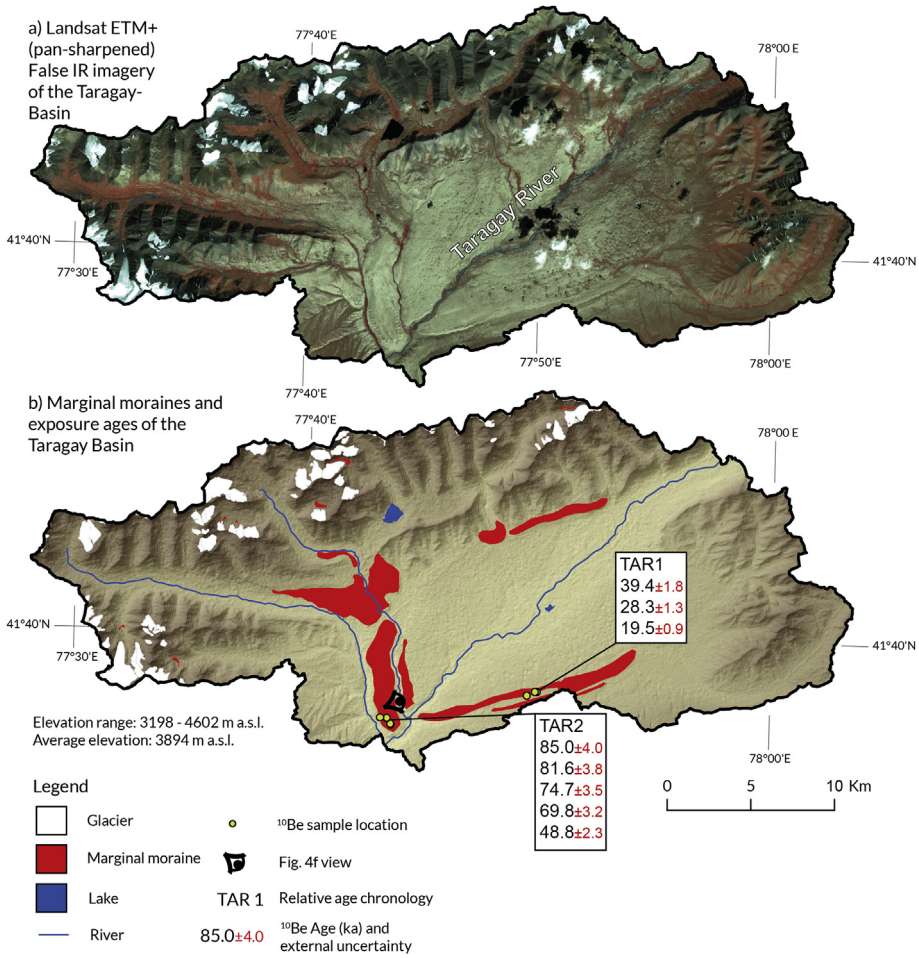

Fig. 7. a) Landsat ETM+ (pan-sharpened) False IR imagery of the Taragay Basin and the Taragay moraine complex. b) Mapped marginal moraines and location of ^{10}Be samples with associated exposure ages (ka). Labels TAR 1 – TAR 2 reflect relative age chronology, 1 being youngest. Location of the figure outline is indicated in Fig. 3. Also shown is Fig. 4f view. (For the figure in colour, the reader is referred to the web version of this article.)

only ~10% of the length of the glacier that deposited TAR 2 (~70 km) further downstream. This pattern, in which most mapped moraines occur inside the valleys of a mountain range, and are absent in downstream basins except for a moraine complex (the Taragay moraines in this case), has been noted in other alpine areas as well (cf. Tibetan Plateau: Owen et al., 2010; Patagonia: Singer et al., 2004). Other studies have shown that the majority of moraines in alpine settings occur within a few tens of percentage of the local maximum ice extent (Kaplan et al., 2009; Anderson et al., 2012). No larger moraine complexes were mapped in valleys or basins beyond the Koyandy Valley (Figs. 3 and 6). However, during fieldwork we noticed the presence of glacial erratics on top of the right-lateral valley interfluve. The glacier depositing this till had to have been significantly thicker (~100 m) than the glacier that deposited KOY 1, the furthest extent mapped in Fig. 6.

6.2. Evaluating the timing of glacier expansions

High-resolution geochronological data is key to a reliable comparison of glacial chronologies across regions and hemispheres (cf. Clark et al., 2009; Shakun et al., 2015). A working methodology to objectively establish deglaciation age uncertainties is therefore an important aspect of defining glacial stages. Fig. 10a illustrates correlation challenges, for example when error margins are too wide to be able to compare local glacial stages across a region. Nevertheless, the Tian Shan glaciers have advanced and retreated many times during the Pleistocene as witnessed by ubiquitous moraine successions in valleys across the mountain system (e.g., Koppes et al., 2008; Zech, 2012; Stroeven et al., 2013; Li et al., 2014; Lifton et al., 2014a). Previous studies comparing and correlating glacial chronologies across the Tian Shan have attempted to show that glacier expansions occurred during MIS 6, 4, and 2 in the eastern and central Tian Shan and during MIS 5 and 3 in the western and southern Tian Shan (Koppes et al., 2008; Xu et al., 2010). Fig. 10a summarises the deglaciation ages of the 25 moraines, analysed in this study. The error ranges for most moraines older than MIS 2 make correlation and linkage to specific marine oxygen isotope stages difficult. If we only consider well- and moderately-clustered deglaciation ages for moraines, we identify moderately-clustered local glacial stages during MIS 5 and 3 and a regional stage during MIS 2 (Fig. 10b). MIS 2 is the only stage identified at more than 1 location, a circumstance that provides ample cause to be cautious about attempting to correlate stages spatially and temporally. Below, we summarise local and regional glacier stages identified across the Tian Shan (Table 2).

6.2.1. The Little ice age

The fact that there are only few studies that have attempted to date Holocene moraines makes the correlation of these glacial stages difficult, if not impossible. Only one Holocene exposure age

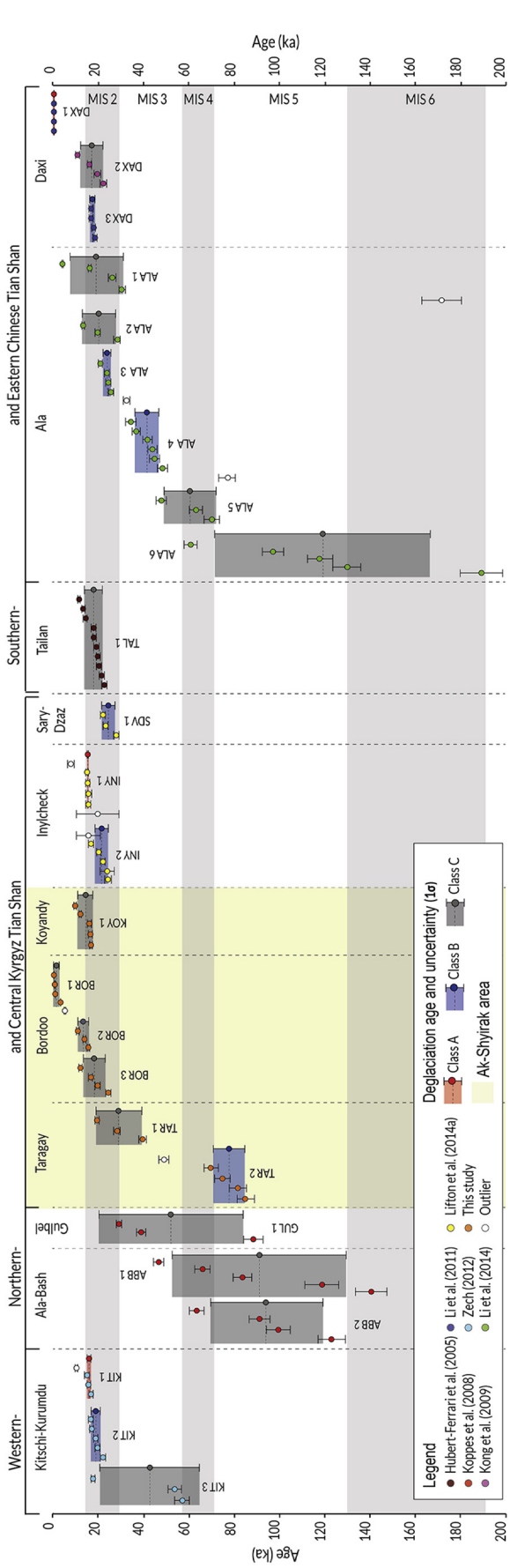

Fig. 8. Tian Shan and Ak-Shyrak area ^{10}Be glacial chronology showing all boulder groups related to marginal moraines with at least 3 samples per moraine and their assignment to exposure age quality classes A, B and C. Sample locations are organized from West to East, and from oldest to youngest in each respective boulder group. Visualised are rejected outliers (non-filled circles) and the quality class (A, B and C) calculated means with uncertainties (standard deviation excluding outliers). (For the figure in colour, the reader is referred to the web version of this article.)

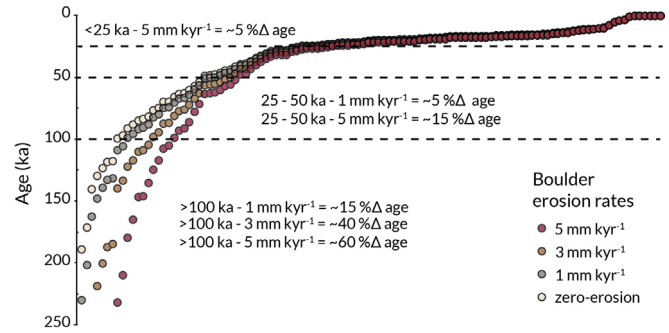

Fig. 9. All ^{10}Be exposure ages in the Tian Shan related to moraines with at least 3 samples (n = 114; see text for references), sorted oldest to youngest, and the effect of boulder erosion rates of 1, 3, and 5 mm kyr^{-1}, using the nuclide specific LSD scaling and the updated global reference production rate of Heyman et al. (2016). (For interpretation of colour in this figure, the reader is referred to the web version of this article.)

group (DAX 1) passed the data quality criteria and yielded a mean exposure age of 0.45 ± 0.03 ka (Li et al., 2014, Fig. 8). Exposure age group BOR 1 is Holocene in age but given the deglaciation age of 1.4 ± 1.3 ka, it was only given a class C quality. This might imply that both of these moraines were deglaciated during the Little Ice Age, but since the BOR 1 age is so poorly constrained this correlation remains inconclusive.

6.2.2. Regional glacial stage 15–28 ka (MIS 2)

Deglaciation ages of the well- and moderately-clustered moraines: INY 1 (15.4 ± 0.3 ka; Lifton et al., 2014a), KIT 1 (15.8 ± 0.9 ka; Zech, 2012), DAX 3 (17.5 ± 1.0 ka; Li et al., 2011), KIT 2 (18.9 ± 2.2 ka; Zech, 2012), INY 2 (21.4 ± 3.1 ka; Lifton et al., 2014a), ALA 3 (23.8 ± 1.9 ka; Li et al., 2014), and SDV 1 (24.4 ± 2.2 ka; Lifton et al., 2014a), all overlap within their uncertainties and coincide with MIS 2 (Figs. 8 and 10). This is the only identified regional glacial stage in the Tian Shan and it is characterised by valley-style glaciation (i.e. paleoglacier extents restricted to valleys) occurring throughout the different sectors of the mountain system. This result is likely robust for a range of boulder erosion rates, since high rates of erosion (5 mm kyr^{-1}), in the <25 ka interval result in at most a ~5% increase in exposure age (Fig. 9).

Deglaciation ages from the class C moraines BOR 2 (13.5 ± 2.2 ka; this study), KOY 1 (14.3 ± 3.1 ka; this study), DAX 2 (17.2 ± 4.9 ka; Kong et al., 2009), TAL 1 (17.9 ± 3.7 ka; Hubert-Ferrari et al., 2005), BOR 3 (18.2 ± 5.1 ka; this study), ALA 1 (19.2 ± 11.7 ka; Li et al., 2014) and ALA 2 (20.4 ± 7.5 ka; Li et al., 2014) are also consistent with deglaciation during MIS 2, although their error margins are wide. We do conclude that deglaciation across the Tian Shan likely occurred between 15 and 28 ka. We reiterate that this age interval is defined as the age range between the minimum and maximum error bounds of individual class A and B moraine deglaciation ages (arithmetic mean and standard deviation of a population of boulders).

We also observe spatial differences in glacier lengths and altitudes across the Tian Shan during MIS 2 (Table 2). In the western sector of the Tian Shan (Kitschi-Kurumdu), glaciers were short (<4 km) and terminated at altitudes of ~3700–3800 m a.s.l. Glaciers in the central sector (Ak-Shyirak and Inylchek) were much more extensive than in the western sector and display a larger variability in length and altitude; the lengths of the Inylchek and Sary-Dzaz paleoglaciers were ~64 and 112 km, extending down to altitudes of 2600 and ~3100 m a.s.l., respectively (Table 2). In the Ala Valley of the eastern Tian Shan the paleoglacier extent was ~6 km from the cirque with a minimum glacier altitude of 3500 m a.s.l. Even though the Inylchek Valley has both an early and late MIS 2 signal recorded

Table 2
Summary of glacial stages inferred from class A and B moraines across the Tian Shan.

Glacial stage	Sector	Group	ID	Deglaciation age (ka)	Uncertainty (ka)	Glacial stage age range (ka)	Altitude glacier margin[a] (m a.s.l.)	Total glacier length[b] (km)
Local	Central	TAR	2	77.8	6.8	71–85	3400	70
Local	Eastern	ALA	4	41.6	5.2	36–47	3100	15
Regional	Central	SDV	1	24.4	3.2	15–28	3100	64
	Eastern	ALA	3	23.8	1.9		3500	6
	Central	INY	2	21.4	3.1		2600	112
	Western	KIT	2	18.9	2.2		3700	4
	Eastern	DAX	3	17.5	1.0		3200	11
	Western	KIT	1	15.8	0.9		3800	3
	Central	INY	1	15.4	0.3		2800	43
Local	Eastern	DAX	1	0.45	0.03	0.42–0.48	3200	1

[a] Altitude glacier margin is determined as the lowest altitude of the terminal moraine of the dated ice advance/deglaciation.
[b] Total glacier length has been estimated from Google Earth as the distance between the lowest altitude of the terminal moraine of the dated ice advance/deglaciation and the headwall of the closest catchment from which the paleoglacier was likely sourced.

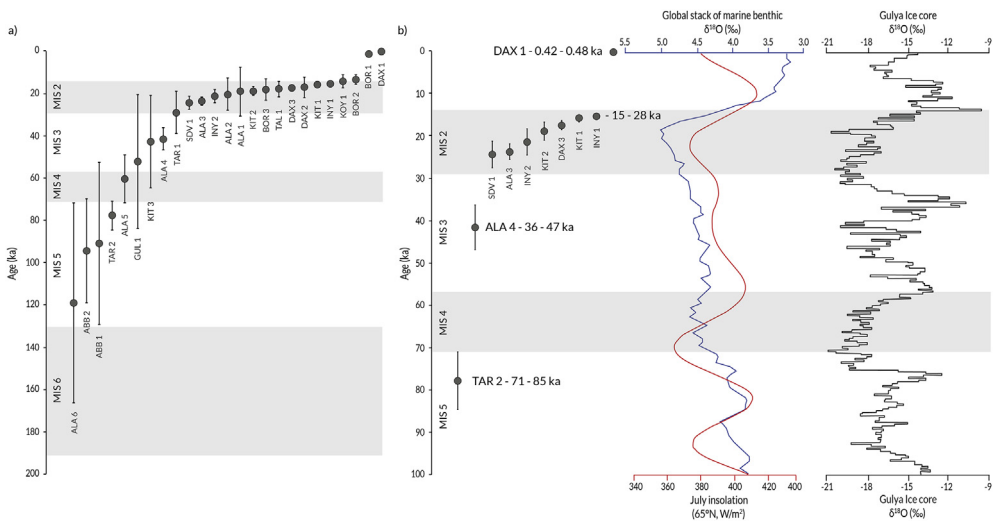

Fig. 10. a) All moraine deglaciation ages and their uncertainties across the Tian Shan and b) selected deglaciation ages from robustly dated moraines in comparison to the Guliya ice core record (Thompson et al., 1997), the global stack of benthic $\delta^{18}O$ (Lisiecki and Raymo, 2005) and July insolation at 65°N (Berger and Loutre, 1991).

in its moraine succession, the neighbouring Sary-Dzaz Valley and the Ala Valley lack a robustly dated late MIS 2 stage for comparison (Fig. 8). The Sary-Dzaz Valley contains a complex sequence of boulder-poor lateral moraines intersected by glacial meltwater channels (Lifton et al., 2014a) so it is very possible that we have yet to identify this equivalent moraine. In the Ala Valley several significant moraines have been mapped and dated but the resolution of the dating control has been too coarse to distinguish sub-stages within MIS 2.

If we consider all MIS 2-dated moraines (including class C) from the central Tian Shan, INY 1, INY 2 and SDV 1 stand out as significant expansions compared to the other moraines. Topographic, topoclimatic, or regional climatic mechanisms could explain the spatial differences in observed glacier extents (Barr and Lovell, 2014). Topographic mechanisms are related to the general valley slope and aspect, valley hypsometry, and elevation of the paleoglacier source area, while topoclimatic mechanisms are associated with orographic precipitation gradients or channeling of precipitation through valley systems (Barr and Lovell, 2014). Regional climatic mechanisms reflect regional cooling or warming, translating into a sequence of moraines (Kirkbride and Winkler, 2012). Because glaciers draining the Jengish Chokusu Massif, the highest area of the Tian Shan, were the most extensive, this likely indicates that topography (catchment size and elevation) is the most important controlling factor/mechanism. More data, however, is needed to differentiate paleoclimatic signals of glacier expansion further from expansions related to local topographic context (section 6.3).

Our analyses provide evidence that paleoglaciers across the Tian Shan retreated between 15 and 28 ka, during MIS 2, implying a general synchronicity with the timing of maximum ice volumes (Clark et al., 2009) and in particular with Northern Hemisphere ice sheets. There is evidence for a final deglaciation across the Tian Shan (KIT 1 and INY 1) occurring later than the onset of Northern Hemispheric deglaciation between 19 and 20 ka (Clark et al., 2009, Fig. 10). But if we take the conservative age range of 15–28 ka, we cannot determine whether paleoglaciers in Tian Shan were leading or lagging behind Northern Hemisphere ice sheet retreats (Dyke, 2004; Kleman et al., 2010; Clark et al., 2012; Hughes et al., 2016; Stroeven et al., 2016).

6.2.3. *Glacial stage 36–47 ka (MIS 3 or older)*

There is only robust evidence for glaciation during MIS 3 in the Ala Valley of the eastern Tian Shan (ALA 4; 41.6 ± 5.2 ka; Li et al., 2014, Figs. 8 and 10). This paleoglacier expanded 15 km downvalley to an altitude of c. 3100 m a.s.l. Even though Koppes et al. (2008) report finding ice expansion during MIS 3 for the central Tian Shan, we cannot confirm such a correlation at this stage across the mountain system. Koppes et al.'s assertion for MIS 3 relies on ages of individual boulders from moraines classified as class C in

the Ala-Bash and Gulbel valleys (ABB 1 and GUL 1, central sector; Fig. 2); our class A and B quality criteria excludes them from this analysis. Other locations sampled in this study by Koppes et al. (2008), were excluded from our analysis because these boulder groups contained <3 boulders. There remains the promise for a more pervasive signal of glaciation during MIS 3 in the Tian Shan to be documented in future studies. A boulder erosion rate of ~5 mm kyr^{-1} gives a mean minimum exposure age of ~48 ka for ALA 4, still positioning this stage within MIS 3. This stage in Ala Valley is thus robust for erosion rates up to ~5 mm kyr^{-1}. With higher erosion rates there is a potential for this stage to be MIS 4.

6.2.4. Missing MIS 4 (57–71 ka)

We have not been able to identify a robust local MIS 4 stage in the Tian Shan, however, individual boulders that fall within this time interval exist in the Ala Valley, the Taragay Basin, and the Ala-Bash and Kitschi-Kurumdu valleys (Fig. 8). A combination of no boulder erosion constraints and a lack of ability to deal with geological uncertainties prohibit us to discuss MIS 4 glacier expansions from the data observed. As discussed above for MIS 3 glacier expansion, there still remains a promise for an MIS 4 signal, but currently we lack the data to support this.

6.2.5. Glacial stage 71–85 ka (MIS 5 or older)

Finally, there is evidence for a local glacial stage during MIS 5 defined by TAR 2 (77.8 ± 6.8 ka; this study; Figs. 8 and 10) in the Taragay Basin. Several glaciers on the southwestern/western slopes of the Ak-Shyirak Massif expanded far below their valley mouths and merged with each other (and with glaciers emanating from the southern slopes of the Terskey Ala Tau Range to the north; Fig. 2) to form a large ice lobe that deposited the TAR 1 and 2 moraines and two local glacial stages can be distinguished in the Taragay Basin. TAR 2 represents the maximum extent of glaciation in the Ak-Shyirak area. The length of the Taragay paleoglacier was ~70 km, measured from the headwall of the Petrov glacier catchment (Fig. 7). The physiography of the Taragay moraines indicates antiquity. The landform has a subtle topographic expression and boulder concentrations are low. If a more pronounced surface expression once existed, it is now all but gone, which could imply that this landform has been subjected to significant surface lowering since formation. Modelling the effects of landform erosion is complex and including boulder erosion rates of 0.1 mm kyr^{-1} increases the age with ~7%, still firmly positioning the minimum landform deglaciation age within MIS 5. A boulder erosion rate of ~5 mm kyr^{-1} pushes the mean minimum exposure age of TAR 2 into MIS 6. This is perhaps not entirely unreasonable, since Lal et al. (2003) report bedrock erosion rates of <30 mm kyr^{-1} from southern and central Tibet. Significant moraine surface lowering would be consistent with the presence of young boulder ages, such as the rejected outlier with an age of 52.9 ± 2.9 ka, due to post-depositional disturbance. Our inability to constrain boulder erosion rates prohibits us to robustly assign this moraine to a specific marine oxygen isotope stage. We consider this stage to be tentative; older glacial deposits typically have larger age uncertainties and it is highly plausible that we have passed the limit for accurate dating because of erosion and exhumation of the landform. TAR 2 might therefore represent extensive glaciation during MIS 6. To extend glacial chronologies beyond MIS 2, there is an urgent need to assign rigorous uncertainties to older moraine deglaciation ages.

6.3. Paleoclimatic implications

Glacier mass balances in the Tian Shan have potentially been influenced by changes in the strengths and locations of three major climatic systems, the Siberian High, the mid-latitude Westerlies and the East-Asian and Indian monsoons (Cheng et al., 2012, Fig. 1). Recent modelling studies have explored the relationship between glacier mass balance and climate at regional scales in Central Asia (Rupper and Roe, 2008; Rupper et al., 2009; Rupper and Koppes, 2009). In general they find that during the early Holocene (Rupper et al., 2009) and at 21 ka (Rupper and Koppes, 2009), in regions where glacier ablation is dominated by melt and surface run off, the pattern of glaciation is mainly due to the patterns in temperature change. Conversely in regions where glacier ablation is dominated by sublimation (i.e. arid regions), glaciers are acutely sensitive to even small changes in atmospheric variables (precipitation and temperature). To further investigate the importance of regional climate differences as drivers for past glaciation, we need widely dispersed and well-dated glaciation records that we can compare with modelling efforts and other proxy records. If glaciers within a region behave similarly at a given point in time we can be confident that regional-scale climate variations exist (Rupper and Roe, 2008). A data quality analysis of the currently available geochronological data (Figs. 8 and 10) has shown that only MIS 2 glaciations, between 15 and 28 ka, are well-dated, widely dispersed, and thus merit paleoclimate analysis, while the paleoclimatic significance of glacier expansions during MIS 3 to 6 should remain more speculative.

In contrast to the Laurentide and Fennoscandian ice sheets, which appear to have grown in size from MIS 5 to MIS 2 (Kleman et al., 1997, 2010); the Barents and Kara ice sheets (Svendsen et al., 1999) and paleoglaciers in the Tian Shan and in north-eastern Eurasia (Barr and Clark, 2012b), became more restricted for each consecutive glaciation after MIS 5. This trend has also been observed in the southern hemisphere in New Zealand (Putnam et al., 2013; Kelley et al., 2014; Doughty et al., 2015; Schaefer et al., 2015) and Patagonia (Darvill et al., 2015b). Fig. 10b compares the timing of regional late MIS 2 glacier retreats with the Gulya $\delta^{18}O$ ice core record from the Kunlun Shan (Fig. 1; Thompson et al., 1997), the global stack of marine benthic $\delta^{18}O$ (Lisiecki and Raymo, 2005), and July insolation at 65°N (Berger and Loutre, 1991). Both the Gulya ice core record and the global stack of marine benthic $\delta^{18}O$ show a peak after 20 ka, following a low in July insolation, and a subsequent glacial-interglacial change in $\delta^{18}O$ reflecting changes towards higher temperatures. Aridity may be one potential reason why MIS 2 glaciers were smaller than previously during the last glacial cycle and that temperature change was the main factor controlling glacier growth at 21 ka (Rupper and Koppes, 2009). Extremely arid conditions in the Tian Shan during MIS 2 have also been inferred as a result of the Fennoscandian Ice Sheet creating an orographic barrier, intensifying the Siberian High, and blocking precipitation carried by the mid-latitude Westerlies (Narama et al., 2007; Koppes et al., 2008; Li et al., 2014). Climate modelling by Krinner et al. (2011) also revealed the effect of moisture-blocking by the western Fennoscandian Ice Sheet during the gLGM, resulting in limited alpine glaciation in eastern Siberia, while allowing for more extensive glaciation at both 70 ka and 140 ka in this region. Paleo-lake records from the Chinese Tian Shan and Inner Mongolia also support arid conditions between 21 and 25 ka coinciding with the gLGM (Wünnemann et al., 2007).

The observed difference in glacier lengths, between 15 and 28 ka, such as more extensive glaciation in the Sary-Dzaz and Inylchek valleys, is likely an effect of local topographic context rather than regional climatic change. For example, most large present-day glaciers draining the Jengish Chokusu Massif have debris-covered snouts. If the investigated paleoglaciers were also debris-covered, this might explain why they were more extensive, because rock-falls on top of glaciers typically cause an advance or surge and might result in the deposition of terminal moraines

(Reznichenko et al., 2011). To investigate this further, the dated moraines across the range need to be complemented with additional well-dated chronologies along west–east and north–south transects, together with detailed sedimentological studies, ruling out any tectonic/rock-fall origin of the dated moraines (Reznichenko et al., 2012). This might also be a possible source of scatter among the surface exposure ages – for example, steep topography and high tectonism.

Evidently, evidence from the Tian Shan seems to indicate limited precipitation and low temperatures during the regional glacial stage 15–28 ka, and thus a northern hemispheric climate signal (weakened Westerly circulation and strengthened Siberian High pressure system). Previous studies have evoked a strengthening of the monsoon to explain earlier more extensive glacier expansions (≥MIS 3) in Tibet and the Himalaya (Dortch et al., 2013; Murari et al., 2014). However, in the Tian Shan, robustly dated glacier limits beyond MIS 2 are still too few to infer regional drivers of glaciation.

7. Conclusions

We have evaluated the timing of former glacier expansions in the Ak-Shyirak area in Kyrgyzstan and across the Tian Shan in Central Asia, by analysing both new and previously published ^{10}Be surface exposure ages of boulders on moraines. Our systematic approach has involved assessments of boulder age scatter on moraines, assignment of boulder group exposure ages to quality classes, and rejection of poorly constrained moraine deglaciation age groups in a regional comparison. This allows us to define and correlate robustly dated glacier limits resulting in a more conservative chronology for use in regional comparisons. In total we analysed 25 moraines with ≥3 boulder ages (n = 114). Based on applied data quality criteria, ~60% of the age data set is deemed to have dominant influences from geological processes, such as inheritance or post-depositional shielding, rendering them inappropriate for regional comparison. Our analysis highlights that we can only confidently define one regional glacial stage, during MIS 2 (15–28 ka). Glacial extents during MIS 2 show that paleoglaciers were mainly restricted to valleys. The restricted extents of these paleoglaciers are interpreted to be the result of arid conditions. Although older exposure ages are to be considered minimum ages, we identified one robust MIS 3 glacier limit in the eastern Tian Shan while MIS 5 glaciation is tentative for the mapped maximum extent of glaciation in the Taragay Basin of the central Kyrgyz Tian Shan. Finally, we conclude that there is no robustly dated evidence for glaciations during MIS 4 or 6, however dated local advances during MIS 3 and especially during MIS 5 might well adhere to these marine stages since we have no control on boulder erosion rates and landform exhumation. Variations in glacier length during MIS 2 are interpreted as a modulation of topography on regional climate. For example, glaciers draining the Jengish Chokusu Massif, the highest area of the Tian Shan, were the most extensive. Such relationships, borne out through robust spatial correlations developed in this study, should motivate intensified research along west– east and north south transects in order to differentiate paleoclimatic signals of glacier expansion from expansions related to local topographic context. With the current resolution and spatial coverage of robustly dated glacier limits we conclude that paleoclimatic implications of the Tian Shan glacial chronology beyond MIS 2 remain speculative.

Acknowledgements

We would like to acknowledge financial support from the Swedish Research Council (No. 2011-4892) to Stroeven and the National Geographic Society to Harbor and Lifton (Grant 9073-12), as well as additional support for field studies from the Swedish Society for Anthropology and Geography (SSAG) and the Margit Alhtin and Carl Mannerfelt stipends to Blomdin and Gribenski. PRIME Lab, Caffee, and Lifton acknowledge support from NSF (EAR-1153689). We received considerable support and help from Tom Clifton and Greg Chmiel at PrimeLab during ^{10}Be sample preparation and processing. We also thank the attendees of the Central Asia Paleoglaciology Project workshops (2011, 2012, 2013) who contributed to some of the ideas and thinking in this paper: Yingkui Li, Alexandru T. Codilean, Krister Jansson, Alexei Rudoy, and Frank Preusser. Adam Stjärnljus, Joakim Ojanen, and Alyona Spuntova are acknowledged for their help during our fieldwork to Kyrgyzstan in 2014. Finally, we thank Christopher M. Darvill and Lewis A. Owen for providing thorough and informative reviews.

Appendix A. Supplementary data

Supplementary data related to this article can be found at http://dx.doi.org/10.1016/j.quascirev.2016.07.029.

References

Abdrakhmatov, K.Y., Aldazhanov, S.A., Hager, B.H., Hamburger, M.W., Herring, T.A., Kalabaev, K.B., Makarov, V.I., Molnar, P., Panasyuk, S.V., Prilepin, M.T., Reilinger, R.E., Sadybakasov, I.S., Souter, B.J., Trapeznikov, Y.A., Tsurkov, V.Y., Zubovich, A.V., 1996. Relative recent construction of the Tien Shan inferred from GPS measurements of presentday crustal deformation rates. Nature 384, 450–453.

Aizen, V., Aizen, E., Melack, J., 1996. Precipitation, melt and runoff in the northern Tien Shan. J. Hydrol 186, 229–251.

Aizen, V., Aizen, E., Kuzmichonok, V., 2007a. Glaciers and hydrological changes in the Tien Shan: simulation and prediction. Environ. Res. Lett. 2, 1–10. http://dx.doi.org/10.1088/1748-9326/2/4/045019.

Aizen, V., Kuzmichenok, V.A., Surazakov, A.B., Aizen, E.M., 2007b. Glacier changes in the Tien Shan as determined from topographic and remotely sensed data. Glob. Planet. Change 56, 328–340. http://dx.doi.org/10.1016/j.gloplacha.2006.07.016.

Anderson, R.S., Dühnforth, M., Colgan, W., Anderson, L., 2012. Far-flung moraines: Exploring the feedback of glacial erosion on the evolution of glacier length. Geomorphology 179, 269–285. http://dx.doi.org/10.1016/j.geomorph.2012.08.018.

Applegate, P.J., Urban, N.M., Laabs, B.J.C., Keller, K., Alley, R.B., 2010. Modeling the statistical distributions of cosmogenic exposure dates from moraines. Geosci. Model Dev. 3, 293–307. http://dx.doi.org/10.5194/gmd-3-293-2010.

Applegate, P.J., Urban, N.M., Keller, K., Lowell, T.V., Laabs, B.J.C., Kelly, M.A., Alley, R.B., 2012. Improved moraine age interpretations through explicit matching of geomorphic process models to cosmogenic nuclide measurements from single landforms. Quat. Res. 77, 293–304. http://dx.doi.org/10.1016/j.yqres.2011.12.002.

Balco, G., 2006. Converting Al and Be Isotope Ratio Measurements to Nuclide Concentrations in Quartz. http://hess.ess.washington.edu/math/docs/common/ams_data_reduction.pdf.

Balco, G., 2011. Contributions and unrealized potential contributions of cosmogenic-nuclide exposure dating to glacier chronology, 1990–2010. Quat. Sci. Rev. 30, 3–27. http://dx.doi.org/10.1016/j.quascirev.2010.11.003.

Balco, G., Stone, J.O., Lifton, N.A., Dunai, T.J., 2008. A complete and easily accessible means of calculating surface exposure ages or erosion rates from ^{10}Be and ^{26}Al measurements. Quat. Geochronol. 3, 174–195. http://dx.doi.org/10.1016/j.quageo.2007.12.001.

Barr, I.D., Clark, C.D., 2009. Distribution and pattern of moraines in Far NE Russia reveal former glacial extent. J. Maps 5, 186–193. http://dx.doi.org/10.4113/jom.2009.1108.

Barr, I.D., Clark, C.D., 2011. Glaciers and climate in Pacific far NE Russia during the last glacial maximum. J. Quat. Sci. 26, 227–237. http://dx.doi.org/10.1002/jqs.1450.

Barr, I.D., Clark, C.D., 2012a. An updated moraine map of Far NE Russia. J. Maps 1–6. http://dx.doi.org/10.1080/17445647.2012.726931.

Barr, I.D., Clark, C.D., 2012b. Late Quaternary glaciations in Far NE Russia; combining moraines, topography and chronology to assess regional and global glaciation synchrony. Quat. Sci. Rev. 53, 72–87. http://dx.doi.org/10.1016/j.quascirev.2012.08.004.

Barr, I.D., Lovell, H., 2014. A review of topographic controls on moraine distribution. Geomorphology 226, 44–64. http://dx.doi.org/10.1016/j.geomorph.2014.07.030.

Benn, D.I., Evans, D.J.A., 2010. Glaciers and Glaciation. Hodder and Arnold, London. http://dx.doi.org/10.2307/1790982.

Benn, D.I., Owen, L.A., 1998. The role of the Indian summer monsoon and the mid-latitude westerlies in Himalayan glaciation: review and speculative discussion. J. Geol. Soc. Lond. 155, 353–363. http://dx.doi.org/10.1144/gsjgs.155.2.0353.

Benson, L., Madole, R., Landis, G., Gosse, J., 2005. New data for Late Pleistocene Pinedale alpine glaciation from southwestern Colorado. Quat. Sci. Rev. 24, 49–65. http://dx.doi.org/10.1016/j.quascirev.2004.07.018.
Berger, A., Loutre, M.F., 1991. Insolation values for the climate of the last 10 million years. Quat. Sci. Rev. 10, 297–317. http://dx.doi.org/10.1016/0277-3791(91)90033-Q.
Blard, P.-H., 2016. Cosmic Ray Exposure Program. http://crep.crpg.cnrs-nancy.fr/#/.
Blomdin, R., Heyman, J., Stroeven, A.P., Hättestrand, C., Harbor, J.M., Gribenski, N., Jansson, K.N., Petrakov, D.A., Ivanov, M.N., Alexander, O., Rudoy, A.N., Walther, M., 2016. Glacial geomorphology of the Altai and western Sayan mountains, central Asia. J. Maps 1–14. http://dx.doi.org/10.1080/17445647.2014.992177.
Bolch, T., 2007. Climate change and glacier retreat in northern Tien Shan (Kazakhstan/Kyrgyzstan) using remote sensing data. Glob. Planet. Change 56, 1–12. http://dx.doi.org/10.1016/j.gloplacha.2006.07.009.
Borchers, B., Marrero, S., Balco, G., Caffee, M., Goehring, B., Lifton, N., Nishiizumi, K., Phillips, F., Schaefer, J., Stone, J., 2016. Geological calibration of spallation production rates in the CRONUS-Earth project. Quat. Geochronol. 31, 188–198. http://dx.doi.org/10.1016/j.quageo.2015.01.009.
Briner, J.P., Kaufman, D.S., Manley, W.F., Finkel, R.C., Caffee, M.W., 2005. Cosmogenic exposure dating of late Pleistocene moraine stabilization in Alaska. GSA Bull. 117, 1108–1120. http://dx.doi.org/10.1130/B25649.1.
Cheng, H., Zhang, P.Z., Spötl, C., Edwards, R.L., Cai, Y.J., Zhang, D.Z., Sang, W.C., Tan, M., An, Z.S., 2012. The climatic cyclicity in semiarid-arid central Asia over the past 500,000 years. Geophys. Res. Lett. 39 http://dx.doi.org/10.1029/2011GL050202 n/a–n/a.
Clark, C.D., Hughes, A.L.C., Greenwood, S.L., Jordan, C., Sejrup, H.P., 2012. Pattern and timing of retreat of the last British-Irish ice Sheet. Quat. Sci. Rev. 44, 112–146. http://dx.doi.org/10.1016/j.quascirev.2010.07.019.
Clark, P.U., Dyke, A.S., Shakun, J.D., Carlson, A.E., Clark, J., Wohlfarth, B., Mitrovica, J.X., Hostetler, S.W., McCabe, a M., 2009. The last glacial maximum. Science 325, 710–714. http://dx.doi.org/10.1126/science.1172873.
Darvill, C.M., Stokes, C.R., Bentley, M.J., Lovell, H., 2014. A glacial geomorphological map of the southernmost ice lobes of Patagonia: the Bahía Inútil – San Sebastián, Magellan, Otway, Skyring and Río Gallegos lobes. J. Maps 10, 500–520. http://dx.doi.org/10.1080/17445647.2014.890134.
Darvill, C.M., Bentley, M.J., Stokes, C.R., 2015a. Geomorphology and weathering characteristics of erratic boulder trains on Tierra del Fuego, southernmost South America: implications for dating of glacial deposits. Geomorphology 228, 382–397. http://dx.doi.org/10.1016/j.geomorph.2014.09.017.
Darvill, C.M., Bentley, M.J., Stokes, C.R., Hein, A.S., Rodés, Á., 2015b. Extensive MIS 3 glaciation in southernmost Patagonia revealed by cosmogenic nuclide dating of outwash sediments. Earth Planet. Sci. Lett. 429, 157–169. http://dx.doi.org/10.1016/j.epsl.2015.07.030.
Desilets, D., Zreda, M., 2003. Spatial and temporal distribution of secondary cosmic-ray nucleon intensities and applications to in situ cosmogenic dating. Earth Planet. Sci. Lett. 206, 21–42. http://dx.doi.org/10.1016/S0012-821X(02)01088-9.
Desilets, D., Zreda, M., Prabu, T., 2006. Extended scaling factors for in situ cosmogenic nuclides: new measurements at low latitude. Earth Planet. Sci. Lett. 246, 265–276. http://dx.doi.org/10.1016/j.epsl.2006.03.051.
Dortch, J.M., Owen, L.A., Caffee, M.W., 2013. Timing and climatic drivers for glaciation across semi-arid western Himalayan–Tibetan orogen. Quat. Sci. Rev. 78, 188–208. http://dx.doi.org/10.1016/j.quascirev.2013.07.025.
Doughty, A.M., Schaefer, J.M., Putnam, A.E., Denton, G.H., Kaplan, M.R., Barrell, D.J.A., Andersen, B.G., Kelley, S.E., Finkel, R.C., Schwartz, R., 2015. Mismatch of glacier extent and summer insolation in Southern Hemisphere mid-latitudes. Geology 43, 407–410. http://dx.doi.org/10.1130/G36477.1.
Dunai, T.J., 2001. Influence of secular variation of the geomagnetic field on production rates of in situ produced cosmogenic nuclides. Earth Planet. Sci. Lett. 193, 197–212. http://dx.doi.org/10.1016/S0012-821X(01)00503-9.
Dyke, A.S., 2004. An outline of North American deglaciation with emphasis on central and northern Canada. Dev. Quat. Sci. 2, 373–424. http://dx.doi.org/10.1016/S1571-0866(04)80209-4.
Dyurgerov, M.B., Mikhalenko, V.N., 1995. Oledeneniye Tien Shanya (Glaciation of Tien Shan). VINITI, Moscow (In Russian).
Farinotti, D., Longuevergne, L., Moholdt, G., Duethmann, D., Mölg, T., Bolch, T., Vorogushyn, S., Güntner, A., 2015. Substantial glacier mass loss in the Tien Shan over the past 50 years. Nat. Geosci. 8, 716–722. http://dx.doi.org/10.1038/ngeo2513.
Fredin, O., Rubensdotter, L., van Welden, A., Larsen, E., Lyså, A., 2012. Distribution of ice marginal moraines in NW Russia. J. Maps 8, 236–241. http://dx.doi.org/10.1080/17445647.2012.708536.
Fu, P., Heyman, J., Hättestrand, C., Stroeven, A.P., Harbor, J.M., 2012. Glacial geomorphology of the Shaluli Shan area, southeastern Tibetan plateau. J. Maps 8, 48–55. http://dx.doi.org/10.1080/17445647.2012.668762.
Fu, P., Harbor, J.M., Stroeven, A.P., Hättestrand, C., Heyman, J., Zhou, L., 2013. Glacial geomorphology and paleoglaciation patterns in Shaluli Shan, the southeastern Tibetan Plateau — Evidence for polythermal ice cap glaciation. Geomorphology 182, 66–78. http://dx.doi.org/10.1016/j.geomorph.2012.10.030.
Glasser, N., Jansson, K., 2008. The glacial map of southern South America. J. Maps 4, 175–196. http://dx.doi.org/10.4113/jom.2008.1020.
Gould, B., 1855. On Peirce's Criterion for the rejection of doubtful observations, with tables for facilitating its application. Astron. J. 4, 81–87.
Grosswald, M.G., Kuhle, M., Fastook, J.L., 1994. Wurm glaciation of lake Issyk-Kul area, tian Shan Mts.: a case Study in glacial history of central Asia. GeoJournal 273–310.
Gribenski, N., Jansson, K., Lukas, S., Stroeven, A., Harbor, J., Blomdin, R., Ivanov, M., Heyman, J., Petrakov, D., Rudoy, A., Clifton, T., Lifton, N., Caffee, M., 2016. Complex patterns of glacier advances during the Lateglacial in the Chagan-Uzun Valley. Russian Altai. Quat. Sci. Rev. 149, 288–305. http://dx.doi.org/10.1016/j.quascirev.2016.07.032.
Hallet, B., Putkonen, J., 1994. Surface dating of Dynamic landforms: young boulders on aging moraines. Science 265, 937–940.
Heyman, J., Hättestrand, C.H., Stroeven, A.P., 2008. Glacial geomorphology of the Bayan har sector of the NE Tibetan plateau. J. Maps 4, 42–62. http://dx.doi.org/10.4113/jom.2008.96.
Heyman, J., Stroeven, A.P., Alexanderson, H., Hättestrand, C., Harbor, J., Li, Y., Caffe, M.W., Zhou, L., Veres, D., Liu, F., Machiedo, M., 2009. Palaeoglaciation of Bayan Har Shan, northeastern Tibetan Plateau: glacial geology indicates maximum extents limited to ice cap and ice field scales. J. Quat. Sci. 24, 710–727. http://dx.doi.org/10.1002/jqs.
Heyman, J., Stroeven, A.P., Harbor, J.M., Caffee, M.W., 2011. Too young or too old: Evaluating cosmogenic exposure dating based on an analysis of compiled boulder exposure ages. Earth Planet. Sci. Lett. 302, 71–80. http://dx.doi.org/10.1016/j.epsl.2010.11.040.
Heyman, J., 2014. Paleoglaciation of the Tibetan Plateau and surrounding mountains based on exposure ages and ELA depression estimates. Quat. Sci. Rev. 91, 30–41. http://dx.doi.org/10.1016/j.quascirev.2014.03.018.
Heyman, J., Applegate, P.J., Blomdin, R., Gribenski, N., Harbor, J.M., Stroeven, A.P., 2016. Boulder height – exposure age relationships from a global glacial ^{10}Be compilation. Quat. Geochronol. 34, 1–11.
Hubert-Ferrari, A., Suppe, J., Van Der Woerd, J., Wang, X., Lu, H., 2005. Irregular earthquake cycle along the southern Tianshan front Aksu area, China. J. Geophys. Res. B Solid Earth 110, 1–18. http://dx.doi.org/10.1029/2003JB002603.
Hughes, A.L.C., Gyllencreutz, R., Lohne, Ø.S., Mangerud, J., Svendsen, J.I., 2016. The last Eurasian ice sheets - a chronological database and time-slice reconstruction, DATED-1. Boreas 45, 1–45. http://dx.doi.org/10.1111/bor.12142.
Jomelli, V., Khodri, M., Favier, V., Brunstein, D., Ledru, M.-P., Wagnon, P., Blard, P.-H., Sicart, J.-E., Braucher, R., Grancher, D., Bourlès, D.L., Braconnot, P., Vuille, M., 2011. Irregular tropical glacier retreat over the Holocene epoch driven by progressive warming. Nature 474, 196–199. http://dx.doi.org/10.1038/nature10150.
Jull, A.J.T., Scott, E.M., Bierman, P., 2015. The CRONUS-Earth inter-comparison for cosmogenic isotope analysis. Quat. Geochronol. 26, 3–10. http://dx.doi.org/10.1016/j.quageo.2013.09.003.
Kaplan, M.R., Hein, A.S., Hubbard, A., Lax, S.M., 2009. Can glacial erosion limit the extent of glaciation? Geomorphology 103, 172–179. http://dx.doi.org/10.1016/j.geomorph.2008.04.020.
Kaplan, M.R., Schaefer, J.M., Denton, G.H., Barrell, D.J.A., Chinn, T.J.H., Putnam, A.E., Andersen, B.G., Finkel, R.C., Schwartz, R., Doughty, A.M., 2010. Glacier retreat in New Zealand during the younger Dryas stadial. Nature 467, 194–197.
Kassab, C., Wang, J., Harbor, J., 2013. Glacial geomorphology of the Dalijia Shan region, northeastern Tibetan plateau. J. Maps 9, 98–105. http://dx.doi.org/10.1080/17445647.2012.754729.
Kelley, S.E., Kaplan, M.R., Schafer, J.M., Andersen, B.G., Barrell, D.J.A., Putnam, A.E., Denton, G.H., Schwartz, R., Finkel, R.C., Doughty, A.M., 2014. High-precision ^{10}Be chronology of moraines in the Southern Alps indicates synchronous cooling in Antarctica and New Zealand 42,000 years ago. Earth Planet. Sci. Lett. 405, 194–206. http://dx.doi.org/10.1016/j.epsl.2014.07.031.
Khromova, T.E., 2003. Late-twentieth century changes in glacier extent in the Akshirak Range, Central Asia, determined from historical data and ASTER imagery. Geophys. Res. Lett. 30, 1863. http://dx.doi.org/10.1029/2003GL017233.
Kirkbride, M.P., Winkler, S., 2012. Correlation of Late Quaternary moraines: impact of climate variability, glacier response, and chronological resolution. Quat. Sci. Rev. 46, 1–29. http://dx.doi.org/10.1016/j.quascirev.2012.04.002.
Kleman, J., Hättestrand, C., Borgström, I., Stroeven, A., 1997. Fennoscandian paleoglaciology reconstructed using a glacial geological inversion model. J. Glac 43, 283–299.
Kleman, J., Jansson, K., De Angelis, H., Stroeven, A.P., Hättestrand, C., Alm, G., Glasser, N., 2010. North American Ice Sheet build-up during the last glacial cycle, 115–21kyr. Quat. Sci. Rev. 29, 2036–2051. http://dx.doi.org/10.1016/j.quascirev.2010.04.021.
Kohl, C.P., Nishiizumi, K., 1992. Chemical isolation of quartz for measurements of in-situ-produced cosmogenic nuclides. Geochim. Cosmochmica Acta 56, 3583–3587.
Kong, P., Fink, D., Na, C., Huang, F., 2009. Late Quaternary glaciation of the Tianshan, Central Asia, using cosmogenic ^{10}Be surface exposure dating. Quat. Res. 72, 229–233. http://dx.doi.org/10.1016/j.yqres.2009.06.002.
Koppes, M., Gillespie, A.R., Burke, R.M., Thompson, S.C., Stone, J., 2008. Late Quaternary glaciation in the Kyrgyz tien Shan. Quat. Sci. Rev. 27, 846–866. http://dx.doi.org/10.1016/j.quascirev.2008.01.009.
Kriegel, D., Mayer, C., Hagg, W., Vorogushyn, S., Duethmann, D., Gafurov, A., Farinotti, D., 2013. Changes in glacierisation, climate and runoff in the second half of the 20th century in the Naryn basin, Central Asia. Glob. Planet. Change 110, 51–61. http://dx.doi.org/10.1016/j.gloplacha.2013.05.014.
Krinner, G., Diekmann, B., Colleoni, F., Stauch, G., 2011. Global, regional and local scale factors determining glaciation extent in Eastern Siberia over the last 140,000 years. Quat. Sci. Rev. 30, 821–831. http://dx.doi.org/10.1016/j.quascirev.2011.01.001.
Kuhle, M., 2011. The high glacial (last ice age and last glacial maximum) ice cover of

high and central Asia, with a critical review of Some recent OSL and TCN dates. In: Ehlers, J., Gibbard, P.L., Hughes, P.D. (Eds.), Quaternary Glaciations - Extent and Chronology. Elsevier Inc. http://dx.doi.org/10.1016/B978-0-444-53447-7.00068-4.

Kutuzov, S., Shahgedanova, M., 2009. Glacier retreat and climatic variability in the eastern Terskey–Alatoo, inner Tien Shan between the middle of the 19th century and beginning of the 21st century. Glob. Planet. Change 69, 59–70. http://dx.doi.org/10.1016/j.gloplacha.2009.07.001.

Lal, D., 1991. Cosmic ray labeling of erosion surfaces: in situ nuclide production rates and erosion models. Earth Planet. Sci. Lett. 104, 424–439. http://dx.doi.org/10.1016/0012-821X(91)90220-C.

Lal, D., Harris, N.B., Sharma, K.K., Gu, Z., Ding, L., Liu, T., Dong, W., Caffee, M.W., Jull, A.J., 2003. Erosion history of the Tibetan Plateau since the last interglacial: constraints from the first studies of cosmogenic ^{10}Be from Tibetan bedrock. Earth Planet. Sci. Lett. 217, 33–42. http://dx.doi.org/10.1016/S0012-821X(03)00600-9.

Li, Y., Liu, G., Kong, P., Harbor, J., Chen, Y., Caffee, M., 2011. Cosmogenic nuclide constraints on glacial chronology in the source area of the Urumqi River, Tian Shan, China. J. Quat. Sci. 26, 297–304. http://dx.doi.org/10.1002/jqs.1454.

Li, Y., Liu, G., Chen, Y., Li, Y., Harbor, J., Stroeven, A.P., Caffee, M., Zhang, M., Li, C., Cui, Z., 2014. Timing and extent of Quaternary glaciations in the Tianger Range, eastern Tian Shan, China, investigated using ^{10}Be surface exposure dating. Quat. Sci. Rev. 98, 7–23. http://dx.doi.org/10.1016/j.quascirev.2014.05.009.

Lifton, N., 2016. Implications of two Holocene time-dependent geomagnetic models for cosmogenic nuclide production rate scaling. Earth Planet. Sci. Lett. 433, 257–268.

Lifton, N.A., Bieber, J.W., Clem, J.M., Duldig, M.L., Evenson, P., Humble, J.E., Pyle, R., 2005. Addressing solar modulation and long-term uncertainties in scaling secondary cosmic rays for in situ cosmogenic nuclide applications. Earth Planet. Sci. Lett. 239, 140–161. http://dx.doi.org/10.1016/j.epsl.2005.07.001.

Lifton, N., Beel, C., Hättestrand, C., Kassab, C., Rogozhina, I., Heermance, R., Oskin, M., Burbank, D., Blomdin, R., Gribenski, N., Caffee, M., Goehring, B.M., Heyman, J., Ivanov, M., Li, Y., Li, Y., Petrakov, D., Usubaliev, R., Codilean, A.T., Chen, Y., Harbor, J., Stroeven, A.P., 2014a. Constraints on the late Quaternary glacial history of the Inylchek and Sary-Dzaz valleys from in situ cosmogenic ^{10}Be and ^{26}Al, eastern Kyrgyz Tian Shan. Quat. Sci. Rev. 101, 77–90. http://dx.doi.org/10.1016/j.quascirev.2014.06.032.

Lifton, N., Sato, T., Dunai, T.J., 2014b. Scaling in situ cosmogenic nuclide production rates using analytical approximations to atmospheric cosmic-ray fluxes. Earth Planet. Sci. Lett. 386, 149–160. http://dx.doi.org/10.1016/j.epsl.2013.10.052.

Lindholm, M.S., Heyman, J., 2015. Glacial geomorphology of the Maidika region, Tibetan plateau. J. Maps 1–8. http://dx.doi.org/10.4113/jom.2011.1161.

Lisiecki, L.E., Raymo, M.E., 2005. A Pliocene-Pleistocene stack of 57 globally distributed benthic δ^{18}O records. Paleoceanography 20, 1–17. http://dx.doi.org/10.1029/2004PA001071.

Lovell, H., Stokes, C.R., Bentley, M.J., 2011. A glacial geomorphological map of the Seno Skyring-Seno Otway-Strait of Magellan region, southernmost Patagonia. J. Maps 7, 318–339. http://dx.doi.org/10.4113/jom.2011.1156.

Menounos, B., Clague, J.J., Clarke, G.K.C., Marcott, S.A., Osborn, G., Clark, P.U., Tennant, C., Novak, A.M., 2013. Did rock avalanche deposits modulate the late Holocene advance of Tiedemann glacier, southern coast mountains, British columbia, Canada? Earth Planet. Sci. Lett. 384, 154–164. http://dx.doi.org/10.1016/j.epsl.2013.10.008.

Molnar, P., Tapponnier, P., 1975. Cenozoic tectonics of Asia: Effects of a continental collision. Science 189, 419–426.

Morén, B., Heyman, J., Stroeven, A.P., 2011. Glacial geomorphology of the central Tibetan plateau. J. Maps 7, 115–125. http://dx.doi.org/10.4113/jom.2011.1161.

Murari, M.K., Owen, L.A., Dortch, J.M., Caffee, M.W., Dietsch, C., Fuchs, M., Haneberg, W.C., Sharma, M.C., Townsend-Small, A., 2014. Timing and climatic drivers for glaciation across monsoon-influenced regions of the Himalayan-Tibetan orogen. Quat. Sci. Rev. 88, 159–182. http://dx.doi.org/10.1016/j.quascirev.2014.01.013.

Narama, C., Kondo, R., Tsukamoto, S., Kajiura, T., Ormukov, C., Abdrakhmatov, K., 2007. OSL dating of glacial deposits during the last glacial in the Terskey-Alatoo range, Kyrgyz republic. Quat. Geochronol 2, 249–254. http://dx.doi.org/10.1016/j.quageo.2006.06.007.

Narama, C., Kondo, R., Tsukamoto, S., Kajiura, T., Duishonakunov, M., Abdrakhmatov, K., 2009. Timing of glacier expansion during the last glacial in the inner tien Shan, Kyrgyz republic by OSL dating. Quat. Int. 199, 147–156. http://dx.doi.org/10.1016/j.quaint.2008.04.010.

Nishiizumi, K., Kohl, C.P., Winterer, E.L., Klein, J., Middleton, R., 1989. Cosmic ray production rates of Be-10 and Al-26 in quartz from glacially polished rocks. J. Geophys. Res. B 94, 907–917. http://dx.doi.org/10.1029/JB094iB12p17907.

Nishiizumi, K., Imamura, M., Caffee, M.W., Southon, J.R., Finkel, R.C., McAninch, J., 2007. Absolute calibration of ^{10}Be AMS standards. Nucl. Instrum. Methods Phys. Res. B 258, 403–413. http://dx.doi.org/10.1016/j.nimb.2007.01.297.

Ochs, M., Ivy-Ochs, S., 1997. The chemical behavior of Be, Al, Fe, Ca and Mg during AMS target preparation from terrestrial silicates modeled with chemical speciation calculations. Nucl. Instrum. Methods Phys. Res. B 123, 235–240. http://dx.doi.org/10.1016/S0168-583X(96)00680-5.

Owen, L.A., Finkel, R.C., Barnard, P.L., Haizhou, M., Asahi, K., Caffee, M.W., Derbyshire, E., 2005. Climatic and topographic controls on the style and timing of Late Quaternary glaciation throughout Tibet and the Himalaya defined by 10Be cosmogenic radionuclide surface exposure dating. Quat. Sci. Rev. 24, 1391–1411. http://dx.doi.org/10.1016/j.quascirev.2004.10.014.

Owen, L.A., Yi, C., Finkel, R.C., Davis, N.K., 2010. Quaternary glaciation of Gurla Mandhata (Naimon'anyi). Quat. Sci. Rev. 29, 1817–1830. http://dx.doi.org/10.1016/j.quascirev.2010.03.017.

Owen, L.A., 2013. Late Quaternary in Highland Asia. In: Elias, S.A. (Ed.), Encyclopedia of Quaternary Science. Elsevier, pp. 236–244. http://dx.doi.org/10.1016/B978-0-444-53643-3.00119-9.

Owen, L.A., Dortch, J.M., 2014. Nature and timing of Quaternary glaciation in the Himalayan-Tibetan orogen. Quat. Sci. Rev. 88, 14–54. http://dx.doi.org/10.1016/j.quascirev.2013.11.016.

Peirce, B., 1852. Criterion for the rejection of doubtful observations. Astron. J. 2, 161–163.

Peirce, B., 1877. On Peirce ' s criterion. Proc. Am. Acad. Arts Sci. 13, 348–351.

Petrakov, D., Shpuntova, A., Aleinikov, A., Kääb, A., Kutuzov, S., Lavrentiev, I., Stoffel, M., Tutubalina, O., Usubaliev, R., 2016. Accelerated glacier shrinkage in the Ak-Shyirak massif, inner tien Shan, during 2003-2013. Sci. Total Environ. 562, 364–378. http://dx.doi.org/10.1016/j.scitotenv.2016.03.162.

Phillips, F.M., Leavy, B.D., Jannik, N.O., Elmore, D., Kubik, P.W., 1986. The accumulation of cosmogenic chlorine-36 in rocks: a method for surface exposure dating. Science 231, 41–43. http://dx.doi.org/10.1126/science.231.4733.41.

Phillips, F.M., Zreda, M.G., Smith, S.S., Elmore, D., Kubik, P.W., Sharma, P., 1990. Cosmogenic chlorine-36 chronology for glacial deposits at bloody canyon, eastern Sierra Nevada. Science 248, 1529–1532. http://dx.doi.org/10.1126/science.248.4962.1529.

Phillips, F.M., Argento, D.C., Balco, G., Caffee, M.W., Clem, J., Dunai, T.J., Finkel, R., Goehring, B., Gosse, J.C., Hudson, A.M., Jull, A.J.T., Kelly, M.A., Kurz, M., Lal, D., Lifton, N., Marrero, S.M., Nishiizumi, K., Reedy, R.C., Schaefer, J., Stone, J.O.H., Swanson, T., Zreda, M.G., 2016. The CRONUS-Earth Project: a synthesis. Quat. Geochronol. 31, 119–154. http://dx.doi.org/10.1016/j.quageo.2015.09.006.

Pieczonka, T., Bolch, T., 2015. Region-wide glacier mass budgets and area changes for the Central Tien Shan between ~1975 and 1999 using Hexagon KH-9 imagery. Glob. Planet. Change 128, 1–13. http://dx.doi.org/10.1016/j.gloplacha.2014.11.014.

Putkonen, J., Swanson, T., 2003. Accuracy of cosmogenic ages for moraines. Quat. Res. 59, 255–261. http://dx.doi.org/10.1016/S0033-5894(03)00006-1.

Putnam, A.E., Schaefer, J.M., Denton, G.H., Barrell, D.J.A., Andersen, B.G., Koffman, T.N.B., Rowan, A.V., Finkel, R.C., Rood, D.H., Schwartz, R., Vandergoes, M.J., Plummer, M.A., Brocklehurst, S.H., Kelley, S.E., Ladig, K.L., 2013. Warming and glacier recession in the rakaia valley, Southern Alps of New Zealand, during Heinrich Stadial 1. Earth Planet. Sci. Lett. 382, 98–110. http://dx.doi.org/10.1016/j.epsl.2013.09.005.

Reznichenko, N.V., Davies, T.R.H., Alexander, D.J., 2011. Geomorphology Effects of rock avalanches on glacier behaviour and moraine formation. Geomorphology 132, 327–338. http://dx.doi.org/10.1016/j.geomorph.2011.05.019.

Reznichenko, N.V., Davies, T.R.H., Shulmeister, J., Larsen, S.H., 2012. A new technique for identifying rock avalanche – sourced sediment in moraines and some paleoclimatic implications. Geology 319–322. http://dx.doi.org/10.1130/G32684.1.

Ross, S.M., 2003. Peirce's criterion for the elimination of suspect experimental data. J. Eng. Technol 20, 1–12.

Rupper, S., Koppes, M., 2009. Spatial patterns in Central Asian climate and equilibrium line altitudes. In: Cléroux, C., Fehrenbacher, J., Phipps, S., Rupper, S., Williams, B., Kiefer, T. (Eds.), IOP Conf. Series: Earth and Environmental Science, pp. 1–7. http://dx.doi.org/10.1088/1755-1315/9/1/012009.

Rupper, S., Roe, G., 2008. Glacier changes and regional Climate: a mass and Energy balance approach. J. Clim 21, 5384–5401. http://dx.doi.org/10.1175/2008JCLI2219.1.

Rupper, S., Roe, G., Gillespie, A., 2009. Spatial patterns of Holocene glacier advance and retreat in Central Asia. Quat. Res. 72, 337–346. http://dx.doi.org/10.1016/j.yqres.2009.03.007.

Schaefer, J.M., Denton, G.H., Kaplan, M., Putnam, A., Finkel, R.C., Barrell, D.J.A., Andersen, B.G., Schwartz, R., Mackintosh, A., Chinn, T., Schluchter, C., 2009. High-frequency Holocene glacier fluctuations in New Zealand differ from the northern Signature. Science 324, 622–625. http://dx.doi.org/10.1126/science.1169312.

Schaefer, J.M., Putnam, A.E., Denton, G.H., Kaplan, M.R., Birkel, S., Doughty, A.M., Kelley, S., Barrell, D.J.A., Finkel, R.C., Winckler, G., Anderson, R.F., Ninneman, U.S., Barker, S., Schwartz, R., Andersen, B.G., Schluechter, C., 2015. The southern glacial maximum 65,000 years ago and its unfinished termination. Quat. Sci. Rev. 114, 52–60. http://dx.doi.org/10.1016/j.quascirev.2015.02.009.

Shakun, J.D., Clark, P.U., He, F., Lifton, N.A., Liu, Z., Otto-Bliesner, B.L., 2015. Regional and global forcing of glacier retreat during the last deglaciation. Nat. Commun. 6, 8059. http://dx.doi.org/10.1038/ncomms9059.

Shi, Y., 2002. Characteristics of late Quaternary monsoonal glaciation on the Tibetan plateau and in East Asia. Quat. Int. 97–98, 79–91. http://dx.doi.org/10.1016/S1040-6182(02)00053-8.

Singer, B.S., Ackert, R.P., Guillou, H., 2004. ^{40}Ar/^{39}Ar and K-Ar chronology of Pleistocene glaciations in Patagonia. GSA Bull. 116, 434–450. http://dx.doi.org/10.1130/B25177.1.

Sorg, A., Bolch, T., Stoffel, M., Solomina, O., Beniston, M., 2012. Climate change impacts on glaciers and runoff in tien Shan (central Asia). Nat. Clim. Chang. 2, 725–731. http://dx.doi.org/10.1038/nclimate1592.

Stone, J.O., 2000. Air pressure and cosmogenic isotope production. J. Geophys. Res. 105, 753–759.

Strelow, F.W.E., Weinert, C.H.S.W., Eloff, C., 1972. Distribution coefficients and anion exchange behavior of elements in oxalic acid-hydrochloric acid mixtures. Anal. Chem. 44, 2352–2356. http://dx.doi.org/10.1021/ac60322a001.

Stroeven, A.P., Hättestrand, C., Heyman, J., Kleman, J., Morén, B.M., 2013. Glacial geomorphology of the tian Shan. J. Maps 9, 505–512. http://dx.doi.org/10.1080/17445647.2013.820879.

Stroeven, A.P., Hättestrand, C., Kleman, J., Heyman, J., Fabel, D., Fredin, O., Goodfellow, B.W., Harbor, J.M., Jansen, J.D., Olsen, L., Caffee, M.W., Fink, D., Lundqvist, J., Rosqvist, G.C., Strömberg, B., Jansson, K.N., 2016. Deglaciation of Fennoscandia. Quat. Sci. Rev. 147, 91–121.

Svendsen, J.I., Astakhov, V.I., Bolshiyanov, D.Y., Demidov, I., Dowdeswell, J.A., Gataullin, V., Hjort, C., Hubberten, H.W., Larsen, E., Mangerud, J., Melles, M., Moller, P., Saarnisto, M., Siegert, M.J., 1999. Maximum extent of the Eurasian ice sheets in the Barents and Kara Sea region during the Weichselian. Boreas 28, 234–242. http://dx.doi.org/10.1111/j.1502-3885.1999.tb00217.x.

Thompson, L.G., Yao, T., Davis, M., Henderson, K., Mosley-Thompson, E., Lin, P.-N., Beer, J., Synal, H.-A., Cole-Dai, J., Bolzan, J., 1997. Tropical climate instability: the last glacial cycle from a Qinghai-Tibetan ice core. Science 276, 1821–1825. http://dx.doi.org/10.1126/science.276.5320.1821.

Tovar, D.S., Shulmeister, J., Davies, T.R., 2008. Evidence for a landslide origin of New Zealand's Waiho Loop moraine. Nat. Geosci. 1, 524–526. http://dx.doi.org/10.1038/ngeo249.

Vaughan, D.G., Comiso, J.C., Allison, I., Carrasco, J., Kaser, G., Kwok, R., Mote, P., Murray, T., Paul, F., Ren, J., Rignot, E., Solomina, O., Steffen, K., Zhang, T., 2013. Observations: cryosphere. In: Stocker, T., Qin, D., Plattner, G.-K., Tignor, M., Allen, S., Boschung, J., Nauels, A., Xia, Y., BEx, V., Midgley, P. (Eds.), Climate Change 2013: the Physical Science Basis. Contribution of Working Group I to the Fifth Assessment Report of the Intergovernmental Panel on Climate Change, pp. 317–382. http://dx.doi.org/10.1017/CBO9781107415324.012.

Wünnemann, B., Hartmann, K., Janssen, M., Zhang Hucai, C., 2007. Responses of Chinese desert lakes to climate instability during the past 45,000 years. Dev. Quat. Sci. 9, 11–24. http://dx.doi.org/10.1016/S1571-0866(07)09003-3.

Xu, X., Kleidon, A., Miller, L., Wang, S., Wang, L., Dong, G., 2010. Late Quaternary glaciation in the Tianshan and implications for palaeoclimatic change: a review. Boreas 39, 215–232. http://dx.doi.org/10.1111/j.1502-3885.2009.00118.x.

Yi, C., Jiao, K., Liu, K., He, Y., Ye, Y., 2002. ESR dating of the sediments of the last glaciation at the source area of the Urumqi river, tian Shan mountains, China. Quat. Int. 97–98, 141–146. http://dx.doi.org/10.1016/S1040-6182(02)00059-9.

Yi, C., Liu, K., Cui, Z., Jiao, K., Yao, T., He, Y., 2004. AMS radiocarbon dating of late Quaternary glacial landforms, source of the Urumqi River, Tien Shan - a pilot study of ^{14}C dating on inorganic carbon. Quat. Int. 121, 99–107. http://dx.doi.org/10.1016/j.quaint.2004.01.026.

Yin, A., 2010. Cenozoic tectonic evolution of Asia: a preliminary synthesis. Tectonophysics 488, 293–325. http://dx.doi.org/10.1016/j.tecto.2009.06.002.

Zech, R., 2012. A late Pleistocene glacial chronology from the Kitschi-Kurumdu Valley, Tien Shan (Kyrgyzstan), based on ^{10}Be surface exposure dating. Quat. Res. 77, 281–288. http://dx.doi.org/10.1016/j.yqres.2011.11.008.

Zhao, J., Zhou, S., He, Y., Ye, Y., Liu, S., 2006. ESR dating of glacial tills and glaciations in the Urumqi River headwaters, Tianshan Mountains, China. Quat. Int. 144, 61–67. http://dx.doi.org/10.1016/j.quaint.2005.05.013.

Zhao, J., Liu, S., He, Y., Song, Y., 2009. Quaternary glacial chronology of the Ateaoyinake river valley, Tianshan mountains, China. Geomorphology 103, 276–284. http://dx.doi.org/10.1016/j.geomorph.2008.04.014.

Zhao, J., Song, Y., King, J.W., Liu, S., Wang, J., Wu, M., 2010. Glacial geomorphology and glacial history of the Muzart river valley, Tianshan range, China. Quat. Sci. Rev. 29, 1453–1463. http://dx.doi.org/10.1016/j.quascirev.2010.03.004.

Zhao, J., Wang, J., Harbor, J.M., Liu, S., Yin, X., Wu, Y., 2015. Quaternary glaciations and glacial landform evolution in the Tailan River valley, Tianshan Range, China. Quat. Int. 358, 2–11. http://dx.doi.org/10.1016/j.quaint.2014.10.029.

Zubovich, A.V., Wang, X., Scherba, Y.G., Schelochkov, G.G., Reilinger, R., Reigber, C., Mosienko, O.I., Molnar, P., Michajljow, W., Makarov, V.I., Li, J., Kuzikov, S.I., Herring, T.A., Hamburger, M.W., Hager, B.H., Dang, Y., Bragin, V.D., Beisenbaev, R.T., 2010. GPS velocity field for the Tien Shan and surrounding regions. Tectonics 29, 1–23. http://dx.doi.org/10.1029/2010TC002772.